



HAL
open science

Extracellular vesicle production and membrane uptake promote repair and antibiotic tolerance in *E. coli*

Julia Bos, Yasmina Abou Haydar, Olena Mayboroda, Pierre-Henri Commere, Didier Mazel

► **To cite this version:**

Julia Bos, Yasmina Abou Haydar, Olena Mayboroda, Pierre-Henri Commere, Didier Mazel. Extracellular vesicle production and membrane uptake promote repair and antibiotic tolerance in *E. coli*. 2025. pasteur-04920024v2

HAL Id: pasteur-04920024

<https://pasteur.hal.science/pasteur-04920024v2>

Preprint submitted on 3 Feb 2025

HAL is a multi-disciplinary open access archive for the deposit and dissemination of scientific research documents, whether they are published or not. The documents may come from teaching and research institutions in France or abroad, or from public or private research centers.

L'archive ouverte pluridisciplinaire **HAL**, est destinée au dépôt et à la diffusion de documents scientifiques de niveau recherche, publiés ou non, émanant des établissements d'enseignement et de recherche français ou étrangers, des laboratoires publics ou privés.

Copyright

1 **Extracellular vesicle production and membrane uptake promote repair and antibiotic**
2 **tolerance in *E. coli***

3
4 **Authors**

5 Julia Bos^{1*}, Yasmina Abou Haydar¹, Olena Mayboroda², Pierre Henri Commere³ and Didier
6 Mazel¹.

7
8 ¹ Institut Pasteur, Université Paris Cité, CNRS UMR3525, Unité Plasticité du Génome
9 Bactérien, 75015 Paris, France

10 ² Institut Pasteur, Université Paris Cité, Biologie des Bactéries Intracellulaires and CNRS
11 UMR 6047, 75724, Paris, France

12 ³ Cytometry platform, Institut Pasteur, Université Paris Cité, Paris, France

13
14 *Corresponding author: julia.bos@pasteur.fr

15
16 **Abstract:**

17 Bacterial extracellular vesicles (EVs) are nanosized lipid structures released in response to
18 environmental stressors, such as phages and antibiotics. Despite their critical role in bacterial
19 adaptability, the mechanisms by which EVs interact with membranes under stress remain
20 poorly understood, due to challenges in visualizing these dynamic processes in live bacteria.
21 Here, we use high-resolution fluorescence microscopy, flow cytometry, and cryo-electron
22 microscopy to investigate EV production and uptake in *Escherichia coli* exposed to sub-
23 minimum inhibitory concentration doses of polymyxin B (Pmb), a membrane-active
24 antimicrobial peptide. Using fluorescently labeled Pmb and EVs, we track Pmb insertion and
25 removal from membranes, EV production and uptake, and their effects on cell growth. Our
26 findings demonstrate that EV production rapidly sequesters Pmb in the medium and facilitates
27 its removal from bacterial membranes. For the first time, we demonstrated that EVs act as
28 membrane plugs by adhering to or fusing with Pmb-damaged membranes. These dynamic
29 processes work together to reduce the antibiotic load from the membranes, turn off the RcsA-
30 mediated membrane stress response, and enable cells to resume growth. Although EVs do
31 not provide resistance to Pmb, they enhance the survival and tolerance of bacterial
32 populations. This study uncovers the dual role of EVs in Pmb sequestration and membrane
33 repair, providing new insights into antibiotic tolerance mechanisms and paving the way for
34 innovative approaches to combat antimicrobial resistance.

35 **Key words** : Extracellular vesicles (EVs), Polymyxin B, EV uptake, Membrane repair,
36 Antibiotic resistance mechanisms.

37
38 **Introduction**

39
40 The world is confronted with the rising threat of bacteria that are resistant to nearly all available
41 antibiotics¹. Antimicrobial peptides (AMPs), such as Polymyxins (i.e. polymyxin B (Pmb) and
42 polymyxin E (colistin)) remain vital antibiotics of last resort due to their efficacy against multi-
43 drug resistant Gram-negative bacteria including critical pathogens² like *Escherichia coli*,
44 *Klebsiella spp.*, and *Pseudomonas aeruginosa*, despite their reported nephro-toxicity^{3,4}. These

45 cationic peptides, originally discovered in *Bacillus polymyxa*⁵ are naturally produced by many
46 organisms as part of their innate defense⁶.

47 The resurgence in the use of polymyxins has spurred research into their mechanisms of action
48 and resistance⁷, which are linked to modifications in lipopolysaccharide (LPS) layer decorating
49 the outer membrane of Gram-negative bacteria⁸ leading to increased efflux, reduced porin
50 pathways and increased membrane blebbing⁹. The discovery of the mobile colistin resistance
51 gene *mcr-1* by Liu et al. in 2016¹⁰ in *Enterobacteriaceae* isolates in China, further revealed the
52 emergence of horizontally acquired resistance genes and thus complicates MDR treatment
53 strategies.

54 Several models describe the interaction of polymyxins, notably Pmb, with bacterial
55 membranes^{11,12}. Pmb initially binds to the negatively charged phosphate group of the lipid A
56 core in the LPS of the outer membrane, neutralizing it¹³. As the peptide progresses to the inner
57 membrane, it disrupts the membrane structure, causing leakage and cell death. Simulation
58 works suggested it loosens LPS packing in the outer membrane while stiffening the inner
59 membrane and promoting membrane adhesion¹⁴. High-resolution AFM studies showed that
60 polymyxins alter *E. coli* surfaces^{15,16} forming hexagonal crystal structures with LPS and
61 divalent cations, leading to increased membrane stiffness, bulging, and rupture¹⁷.

62 The membrane-disrupting effects of Pmb trigger several conserved membrane stress
63 responses¹⁸ that enable bacteria to adapt to the antibiotic stress¹⁹. In *E. coli* and other bacteria,
64 the sigma E pathway and Cpx two-component system²⁰, manage misfolded proteins and
65 repair membrane damage, while the Rcs two-component pathway regulated by RscC, RcsA
66 and RcsB, responds to envelope stress affecting the outer membrane and peptidoglycan
67 layer^{21–24}. Additionally, some bacteria employ PhoP/PhoQ²⁵ and PmrA/PmrB^{26,27} systems to
68 modify their outer membrane under polymyxin exposure.

69 Beyond these intrinsic mechanisms, extracellular vesicles (EVs) have emerged as key
70 mediators involved in the development of antimicrobial resistance (AMR)²⁸. These nanosized
71 lipid-enclosed particles, released in response to stress, sequester antibiotics and protect
72 bacterial populations by reducing local antibiotic concentrations and shielding cell membranes
73^{30–35}. In particular, EVs have been implicated in polymyxin resistance^{30–36} in microorganisms
74 like *E. coli*^{30,37}, *A. baumannii*³³, *P. syringae*³², *S. Typhi*³⁵, and *P. aeruginosa PAO1*³⁴ in which
75 EV production mitigates immediate antibiotic stress by sequestering the Pmb, colistin or
76 melittin drugs. Notably, EVs purified from Pmb-resistant strains protect MDR strains against
77 the bactericidal effect of Pmb^{30,33}, suggesting that EVs extend the spectrum of drug resistance.

78 Despite growing evidence for the role of EVs in antibiotic tolerance, critical questions remain
79 about their direct interactions with bacterial membranes. Current models emphasize EV-
80 mediated drug sequestration, but the potential for EV uptake into membranes, particularly as
81 a repair mechanism, remains unexplored. Unlike eukaryotic cells, where protein complexes
82 mediate vesicle fusion^{39–42} the analogous processes in bacteria are less defined. Some studies
83 suggest ESCRT-like proteins may play a role in bacterial EV dynamics⁴³, but their function in
84 vesicle formation, release, or membrane fusion remains speculative and more research is
85 needed to capture fusion events and to identify potential fusion machinery.

86 Here, we investigated the real-time interplay between EVs, Pmb, and stressed bacteria
87 under sub-minimum inhibitory concentration (sub-MIC) doses of polymyxin B. By combining
88 high-resolution fluorescence microscopy, flow cytometry, and cryo-electron microscopy, we
89 uncover a novel role for EVs as membrane repair agents. We show that EVs not only
90 sequester Pmb from damaged membranes but also adhere to and fuse with bacterial
91 membranes, alleviating envelope stress and promoting tolerance. These findings provide the
92 first direct evidence of EV uptake into bacterial membranes emphasizing the importance of
93 single-cell studies in uncovering bacterial adaptation to antibiotic stress.

94 **Results**

95

96 ***E. coli* bacteria trigger membrane stress response and develop tolerance to sub-** 97 **inhibitory doses of Polymyxin B within hours.**

98 We explored the role of EVs produced by live *E. coli* bacteria exposed to sub-minimum
99 inhibitory concentration (sub-MIC) doses of polymyxin B (Pmb), a membrane-active antibiotic.
100 Growth curves of wild-type (wt) bacteria in LB medium showed that the cells exposed to sub-
101 inhibitory concentrations of Pmb (0.25x and 0.5x MIC) resumed growth after 150 minutes and
102 360 minutes respectively, whereas they were killed with no emergence of growth at a high
103 dose of Pmb (1xMIC) (Figure 1A). This suggests that wt cells, within hours, adapted to sub-
104 inhibitory concentrations of Pmb. We thus investigated the mechanisms underlying this
105 adaptation. Whole genome sequencing of these adapted populations revealed no mutations
106 in their genomes (see “*Methods*”), indicating that the bacteria have developed tolerance and
107 not resistance to the drug. In addition to our sequencing results, we conducted growth assays
108 on the adapted populations, those capable of growing after prolonged exposure to 0.5x MIC
109 Pmb but susceptible to lethal concentrations. These assays revealed that the adapted
110 populations exhibit increased tolerance to sub-MIC levels of Pmb compared to naïve cells
111 exposed to the drug, while still being killed at higher doses (Figure 1B).

112 To probe the impact of polymyxin B (Pmb) on cellular physiology, we measured
113 membrane stress levels using a GFP fusion reporter for the *rcaA* gene. RcsA is part of the
114 Rcs regulon, a two-component system that detects envelope stress and peptidoglycan
115 perturbations^{23,24}, which can be triggered by Pmb. We observed a 3-fold, 5-fold, and 9-fold
116 increase in *rcaA-gfp* expression following the addition of Pmb at 0.25x, 0.5x, and 1x MIC,
117 respectively (Figure 1C). This induction was further confirmed through snapshot images taken
118 60 minutes post-treatment using single-cell fluorescence microscopy (Figure 1D) and flow
119 cytometry analysis (Figure 1E and Figure S1).

120

121 **Production of extracellular vesicles turn off the membrane stress response induced** 122 **by sub-inhibitory doses of Pmb.**

123 Another layer of the Pmb-induced membrane stress response is the production of EVs
124 released into the microenvironment^{30,44}. Yet, the effects of sub-MIC Pmb doses on EV
125 production and on bacterial physiology have been largely overlooked.

126 We measured and showed that EV production increased with sub-MIC concentrations of Pmb
127 and with the duration of exposure to the drug (Figure 1F). Specifically, endogenous EV
128 production increased by 23 (± 16) fold within the first hour of Pmb (0.5x MIC) exposure, 30
129 (± 13) fold after 4 hours, 36 (± 16) fold after 6.5 hours, and 84 (± 26) fold after 20 hours. The
130 increase in EV production at 6.5 hours (400 minutes) which corresponds to 1.5×10^{10} (± 5.7

131 $\times 10^9$) EVs (per ml) coincided with the growth restart observed in Figure 1A and suggests that
132 such concentration of EVs is sufficient to help the cells cope with Pmb (0.5x MIC) and resume
133 proliferation.

134 Furthermore, the production and accumulation of EVs upon Pmb exposure also
135 correlate with suppression of the membrane stress response, as indicated by reduced *rscA-*
136 *gfp* expression levels from ~ 500 minutes to the end of the experiment (Figure 1C).

137 Consistent with a previous study by Manning and Khuen³⁰ the addition of pure EVs
138 concomitantly to Pmb, at a concentration of (~ 8 to 160 EV per cell) at near-physiological
139 production levels (~ 4 to 111 EV per cell) (see *Methods* and Table S2) facilitated immediate
140 growth restoration (Figure 1A), regardless of the type and origin of EVs (Figure S2 AB). Most
141 importantly we showed that rapid growth resumption in the presence of pure EVs occurs by
142 maintaining *rscA-gfp* expression levels to basal levels, preventing cells from entering a
143 stressed state (Figure 1C). Microscopy images and flow cytometry quantification of *rscA-gfp*
144 expression levels in single cells confirmed the basal expression of *rscA-gfp* when pure EVs
145 were added (Figure 1D-E).

146 Next, we showed that the efficacy of EVs in restoring growth depends on the
147 concentration and type of antibiotics, whether they are membrane-active antibiotics (Pmb,
148 Colistin) or non-membrane-targeting antibiotics (Cip, Tobra) (Figure S3). Pure EVs effectively
149 restored the growth of wt bacteria treated with lethal doses of Pmb and colistin, whereas EV
150 addition effect is limited or negligible in the presence of sub-MIC doses of Tobra (a translation-
151 inhibitory antibiotic) and Cip (a DNA-damaging antibiotic) (Figure S3).

152

153 **Fluorescent Polymyxin B (Pmb_{fl}) efficiently binds to cell membranes and triggers RcsA-** 154 **dependent envelop stress response**

155 To gain knowledge on the mechanisms underlying Pmb tolerance at the single cell level, we
156 studied the interaction between the antibiotic, the EVs and the bacteria by using a fluorescent
157 derivative of polymyxin B (which we named Pmb_{fl}), that is conjugated to the fluorescent dye,
158 Rhodamine B. We determined that the MIC of this Pmb derivative is at 8 $\mu\text{g/ml}$ (Figure 2A). At
159 subMIC concentrations of 0.4x and 0.8x MIC (Figure 2A), growth resumed at later times, 180
160 minutes and 450 minutes, respectively, indicating the emergence of tolerance similar to that
161 was observed with plain Pmb. Upon incubation with Pmb_{fl} (0.5x MIC) the fluorescently labeled
162 drug localized rapidly to the bacterial membranes (Figure 2B) and the majority of wt bacteria
163 (97.8% ± 0.33) exhibited positive Pmb_{fl} staining (Figure 2C and Figure S4 AB) within 30
164 minutes.

165 We monitored *rscA-gfp* expression levels in wt cells in the presence of Pmb_{fl} and found
166 that Pmb_{fl} efficiently activates RcsA-dependent membrane stress response, both at the
167 population level (prolonged Pmb_{fl} exposure) (Figure 2D) and in individual cells (30 minutes
168 Pmb_{fl} exposure)(Figure 2E and Figure S4 CD). Using two-color imaging and flow cytometry,
169 we analyzed antibiotic-targeted cells (Pmb_{fl}⁺) and the stress response marker (*rscA-gfp*) after
170 30 minutes of Pmb_{fl} exposure We showed that the membrane stress signal colocalizes with
171 antibiotic trapping in the cell membranes of 24.5% ± 3.8 of the population while 75.2% ± 3.4
172 are positively decorated with the drug but have not triggered the membrane stress response
173 yet (Figure 2F and Figure S4 CD). Altogether, Pmb_{fl} proves to be an effective tool for
174 investigating the mechanisms linked to Pmb tolerance.

175

176

177 **EVs production quickly sequesters Pmb_{fl} and facilitates antibiotic clearance from the**
178 **bacterial membranes**

179 Interestingly, adding pure EVs in a delayed manner (30, 60 or 120 minutes following Pmb
180 addition) to the culture, enabled growth restoration and emergence of drug tolerance, yet with
181 an increased lag phase before growth resumption (Figure 3A). This suggests that EV-
182 mediated mechanisms of antibiotic tolerance extend beyond a simple decoy effect.

183 To understand these mechanisms we examined the dynamics of EV interaction with the
184 antibiotic and bacterial cell membranes through a time-course experiment using Pmb_{fl}. We
185 incubated cells with Pmb_{fl} and collected samples over time (0, 30, 60, 120, 240 and 1200
186 minutes). At each time point, cells were centrifuged, and the fluorescent signal of Pmb_{fl} was
187 analyzed in both the pellet fractions (i.e. cell membranes) (Figure 3B) and the supernatant
188 (containing EVs) (Figure 3C) of cell populations, and in single cells (Figure 3EFG). This assay
189 was performed on 3 strains: wt, *ompA* (that lacks the outer membrane porin OmpA and shows
190 an hypervesiculating phenotype), and wt cells supplemented with pure EVs at a dose at near-
191 physiological production levels. The use of the *ompA* strain is relevant because it produces
192 ~20 times more vesicles than a wt strain in the absence of antibiotics (Figure 3D), while the
193 strains display a similar growth and survival rate (Figure S5). In wt cells, Pmb_{fl} rapidly
194 accumulated in the cell membranes, as shown by a sharp increase in fluorescence signal in
195 the pellet fraction, peaking at 30 minutes (Figure 3B and 3E). This signal then gradually
196 decreased, possibly due to cell division that dilutes the signal in the cell membranes (Figure
197 3B and 3E). Meanwhile, by 60 minutes and throughout (120, 240 and 1200 minutes) Pmb_{fl}
198 signal started to accumulate in the supernatant, indicating the production of vesicles that have
199 sequestered the drug, eventually remaining free in the intercellular space, or bound to
200 membranes (Figure 3B and 3E). These processes of antibiotic trapping and clearance via
201 vesiculation, were augmented in the hypervesiculating cells (*ompA*) (Figure 3B, 3C and 3F).
202 The *ompA* strain exhibited increased accumulation of Pmb_{fl} in the supernatant from time 120
203 minutes (Figure 3C and 3F) that correlates with a decrease in Pmb_{fl} signal from the cell
204 membranes (Figure 3B and 3F).

205 In contrast, the simultaneous addition of pure EVs and Pmb_{fl} resulted in rapid antibiotic
206 neutralization by the EVs (within seconds) (Figure 3C and 3G), and significantly reduced Pmb_{fl}
207 access to the cell membranes throughout the experiment (Figure 3B and 3G), confirming the
208 EV-mediated decoy effect previously reported by other groups^{30,33}

209 Next, we investigated the role of vesiculation in membrane repair and growth restart
210 by monitoring Pmb_{fl} decay associated with membrane damage recovery and subsequent cell
211 growth (Figure 3H-K). In this experiment, wt and *ompA* cells were exposed to sub-MIC Pmb_{fl}
212 for 60 minutes followed by removal of excess antibiotic by centrifugation and resuspension of
213 the cell pellets in fresh medium. Thus, the initial fluorescence signal from Pmb_{fl} originates from
214 the cell pellets and we measured the cells' ability to clear the antibiotic through vesiculation
215 (Figure 3H, 3J and 3K). Time-course analysis revealed that wt cells showed slower Pmb_{fl}
216 elimination from their membranes and delayed growth recovery compared to
217 hypervesiculating *ompA* cells. Fluorescence imaging of single cells indicated the decay of
218 Pmb_{fl} signal intensity in the cell membranes both in wt and *ompA*, which occurred
219 concomitantly with cell division restart (~ 60 minutes), microcolony formation, and the release
220 of EVs (Movie S1 and S2) from cell membranes. Growth resumption proved more efficient in
221 *ompA* (Figure 3I), with less cell-cell variability (Figure 3I and 3K), likely due to an increased
222 rate of membrane repair associated with EV release (Figure 3F and 3G bottom and movie

223 S2). These results align with *ompA* cells showing a survival advantage over wild-type cells in
224 the presence of sub-MIC Pmb (Figure S5).

225 In conclusion, these single-cell studies highlight that EV production promotes the
226 sequestration and clearance of antibiotics like Pmb_{fil} from bacterial membranes enabling
227 membrane repair and growth recovery upon Pmb stress.

228

229 **EV uptake facilitates membrane repair and enhances growth recovery of stressed** 230 **bacteria**

231 In the following experiments, we explored whether EVs could be taken up by the bacteria as
232 membrane patches to repair damaged membranes. To test this, we purified fluorescently
233 labeled EVs using the lipophilic dye (FM 1-43) which integrates into the lipid bilayer of the EV
234 membrane. For these experiments, wt cells were exposed to Pmb (0.5x MIC for 30 minutes)
235 before adding fluorescent EVs (EV_{Green}) for a short incubation time (10 minutes). Excess
236 EV_{Green} and Pmb were subsequently removed by centrifugation. Combining microscopy, flow
237 cytometry, and cryo-electron tomography, we provide the first evidence that EVs can associate
238 with the membranes in real time and be taken up by the cell membranes of wild-type cells
239 upon Pmb antibiotic exposure (Figure 4A-D and Figure S6). In the absence of antibiotic drugs,
240 little to no EV_{Green} uptake (1.5%) was observed and measured in single cells (Figure 4A and
241 4B and Figure S5). In contrast, EV_{Green} uptake significantly increased in cells challenged with
242 Pmb (15%) and Colistin (65%), both membrane-targeting antibiotics (Figure 4B and Figure
243 S6), but not with cipro (2.5%), a DNA replication inhibitor molecule (Figure 4B and Figure S6).
244 We also showed that EVs loaded with Pmb (EV_{PmbGreen}) (which exhibit a slightly smaller
245 diameter; Figure S7), or loaded with Pmb_{fil}, can be taken up by 10% to 50% of wt cells treated
246 with Pmb and Colistin respectively (Figure 4B, Figure S8A-D), suggesting that antibiotic-
247 loaded EVs may have an affinity for damaged membranes and/or play an active role in
248 membrane repair. Altogether, these findings indicate that EV uptake depends on the type of
249 antibiotic and is promoted by membrane-active antibiotics.

250

251 We used cryo-electron microscopy (cryo-EM) to capture details of EVs' interaction with
252 *E. coli* cell membranes. Cryo-EM enables high-resolution imaging of biological samples in their
253 near-native state by preserving delicate membrane structures without chemical fixation,
254 minimizing artifacts. It is ideal for capturing dynamic processes like vesicle docking and fusion.
255 The electron micrographs we obtained, are shown in Figure 4CD and Figure S9. We observed
256 that in the absence of Pmb, EVs remain at a distance with the membrane of *E. coli* cells (Figure
257 4C and movie S3). In contrast, in the presence of Pmb, more EVs adhere to the cell
258 membrane, and in some places were captured fusing with the outer membrane (Figure 4D,
259 Figure S9 and movie S4).

260

261 Next, we asked whether stressed bacteria (*rcsA-gfp*⁺) are more likely to take up EVs
262 compared to non-stressed individuals (*rcsA-gfp*⁻). We used flow cytometry analysis with our
263 two-color imaging setup to simultaneously monitor envelope stress (*rcsA-gfp*) and EV uptake
264 (EV_{Red}) in single cells (Figure 4EF and Figure S8EF). Our data revealed that EV uptake was
265 notably higher in the stressed subpopulation (72% ± 5.8) compared to non-stressed bacteria,
266 which exhibited 19.7% ± 0.8 uptake (Figure 4F). The latter could represent dead cells (as seen
267 in our microscopy images Figure 4E) or persister cells that may not trigger a stress response

268 despite having their membranes prone to take up EVs. We also observed a small subset of
269 stressed cells (5.6% \pm 4.2) that did not efficiently take up EVs (Figure 4F). These results
270 suggest that the nature of the recipient cells plays a critical role in determining EV uptake
271 under stress conditions.

272 Last, to assess if EV uptake plays a role in the development of Pmb tolerance, we
273 determined whether the subpopulations of EV-patched cells, recover growth more efficiently
274 than unpatched subpopulations. We cell sorted fluorescently positive (*rcaA-gfp*⁺ (green⁺),
275 *EV_{red}*(red⁺), *rcaA-gfp*⁺ +*EV_{red}* (green⁺red⁺) and not fluorescent subpopulations (unstained)
276 (Figure 4G and Figure S10) from wt pPr*rcaA-gfp* cells exposed to Pmb and pure *EV_{red}*, and
277 compared their growth recovery after Pmb removal (Figure 4H). We sorted the subpopulations
278 into EV-patched cells (18%, consisting of 12% stressed and 5.2% non-stressed bacteria) and
279 non-patched cells (73%, consisting of 40% stressed and 30% non-stressed bacteria) (Figure
280 4G). Surprisingly, the EV-patched subpopulations, regardless of their membrane stress levels,
281 exhibited rapid growth recovery. They entered the exponential phase at about 250 minutes
282 after a significant lag phase, similar to the unstained cells. However, the non-EV-patched
283 stressed bacteria exhibited a prolonged lag phase and resumed growth only after about 400
284 minutes (Figure 4H).

285 Altogether, our results demonstrated that EVs can be taken up by *E. coli* bacteria upon Pmb
286 stress and serve as repair entities by adhering and/or fusing with damaged cell membranes.
287 This enables stressed cells to resume growth and enhance their tolerance to Pmb antibiotic.

288 Discussion

289 The rising threat of antibiotic-resistant bacteria has heightened interest in antimicrobial
290 peptides (AMPs) like polymyxins, which remain effective against many MDR Gram-negative
291 bacteria^{1,9}. Polymyxins, such as Pmb and Colistin, disrupt the bacterial membrane by targeting
292 its LPS layer. However bacteria have evolved strategies to tolerate or resist these effects⁷.
293 EVs play a key role in bacterial adaptation by transferring genetic material, proteins, and
294 metabolites, aiding survival under stressors like antibiotics²⁸. EVs can act as decoys to
295 sequester polymyxins, reducing their efficacy³⁰⁻³⁵. Despite these roles, the mechanisms by
296 which EVs interact with bacterial membranes in response to antibiotic stress remain unclear,
297 emphasizing the need for alternative approaches to study the complex interplay between EVs,
298 bacteria, and antibiotics.

299 In this work, we combined fluorescence microscopy, flow cytometry, and cryo-electron
300 microscopy to study the real-time dynamics of interactions between *E. coli* bacteria, EVs, and
301 fluorescent Pmb. By labeling Pmb and EVs, we tracked drug insertion, removal, EV
302 production, and uptake, as well as their effects on cell stress response and survival. Our
303 findings reveal that EV production and EV uptake work together to repair damaged
304 membranes, with EVs acting as membrane plugs, to alleviate envelope stress, and enable
305 growth recovery (Figure 5). Our results uncover novel functions of EVs in repairing cell
306 membranes and promoting tolerance to membrane-active antibiotics.

307 We used a fluorescent version of Pmb, Rhodamine-Pmb that we named Pmb_{fl} to investigate
308 the temporal and spatial aspects of Pmb insertion and cell response. While Pmb_{fl} showed an
309 increased MIC (8 μ g/ml) compared to the original Pmb (2 μ g/ml) (Figure 2A), it effectively

310 impaired the growth of wt cells (Figure 2D) and activated the RcsA-mediated membrane
311 stress response in 30% of the population after 30 minutes of exposure (Figure 2EF). Pmb_{fl}
312 also robustly stained the membranes of wt cells, with most cells (99%) becoming Pmb_{fl}-
313 positive within 30 minutes of incubation (Figure 2BC, Figure 3B and 3E) proving the efficacy
314 of binding of the drug. Notably, the heterogeneity in RcsA expression (Figure 2EF) and division
315 rates observed after Pmb_{fl} removal (Figure 3IJ) suggests potential differences in membrane
316 properties or membrane stress thresholds, which may represent biologically significant
317 survival strategies.

318 We observed that EV production facilitates the clearance of Pmb_{fl} from cell membranes as
319 early as 90 minutes after its addition (Figure 3B, 3C, and 3E). EV-bound Pmb_{fl} accumulated
320 more sharply during the late logarithmic phase (120-250 minutes) than in the early stationary
321 phase (250-1200 minutes)(Figure 3C), suggesting that actively dividing cells prioritize the
322 removal of membrane-bound Pmb through EV release as opposed to non-dividing or
323 metabolically slower cells, where the demand for recovery mechanisms might be lower. This
324 finding aligns with previous studies showing that vesicle production peaks during cell division
325 in the Gram-negative bacteria like *E. coli* and *B. melitensis*^{45,46}.

326 To further investigate EV-mediated drug clearance, we studied *ompA* mutant cells, which
327 produce approximately 20 times more EVs than wild-type cells (Figure 3D and table 2).
328 Notably, *ompA* cells accumulated less Pmb_{fl} in their membranes (Figure 3B) and exhibited
329 faster and more efficient membrane drug clearance and growth recovery following drug
330 removal (Figure 3C, 3I and 3K). One possible explanation for the observed increase in Pmb
331 tolerance in the absence of OmpA (Figure S5) is a modification in the lipid A structure.
332 However, previous work ⁴⁷ has shown that the lack of OmpA does not directly alter lipid
333 composition or membrane integrity under non-stress conditions. Instead, OmpA deficiency
334 primarily affects membrane permeability and stability by disrupting its structural interactions
335 with the peptidoglycan (PG) layer. These findings suggest that the increased tolerance to Pmb
336 may involve additional mechanisms, and raise the question of whether *ompA*-derived EVs are
337 more effective at sequestering Pmb, potentially due to differences in their surface properties
338 or lipid composition.

339 Using fluorescence microscopy combined with flow cytometry, we showed that 15–60% of
340 cells take up fluorescently labeled EVs under sub-MIC levels of Pmb and Colistin (Figures 4A
341 and 4B, 4EF). EV uptake increases up to 50 % in the presence of Pmb-loaded EVs (Figure
342 4B and S8A-D). In microscopy images, EV uptake was very well evidenced by discrete
343 fluorescent foci spread along the cell contours, representing EV-cell membrane interactions.
344 To our knowledge, this is the first direct evidence of bacterial EV fusion events captured in
345 real-time at the single-cell level. It will be interesting to further understand whether specific
346 subpopulations of EVs are more efficient for uptake, based on their lipid properties and/or
347 sizes.

348 In support of these findings, our cryo-electron micrographs provide high-resolution visual
349 evidence of EV interactions with cell membranes under Pmb stress, including EV fusion with
350 the outer membrane (Figure 4D, Movie S4). By introducing a centrifugation step to remove
351 nascent EVs from the cell surface, we confirmed that the observed EV-membrane interactions

352 represent uptake events rather than release. A complementary challenging technique such as
353 correlative light and electron microscopy (CLEM) could further validate these findings and
354 elucidate the dynamics of EV-bacterial membrane interactions.

355 Our cell sorting and growth analysis revealed that stressed cells patched with EVs resumed
356 growth faster than those without EV patches, emphasizing the critical role of EV-mediated
357 intermembrane fusion in membrane repair and growth recovery (Figure 4H). Beyond growth
358 resumption, it remains to be determined whether EV uptake also restores other cellular
359 functions, such as metabolism or intracellular organization. Additionally, our data suggest that
360 cells with moderate to severe membrane stress are primed for higher EV uptake (Figure 4EF).
361 Investigating whether the repair mechanism operates randomly or selectively and how donor
362 and recipient cell properties influence this process will provide deeper insights into EV-
363 mediated communication and its role in antibiotic resistance.

364 These findings highlight the importance of single-cell studies in uncovering bacterial
365 adaptation mechanisms to antibiotic stress. By revealing the dual role of EVs in membrane
366 repair and Pmb sequestration, this work provides new insights into the mechanisms underlying
367 Pmb tolerance, an antibiotic of critical public health concern. This study paves the way for
368 innovative approaches to combat antimicrobial resistance, including precision therapies
369 targeting EV production and fusion in stressed bacterial populations.

370 **Methods**

371 **Bacterial strains and growth media.**

372 The bacterial strains used in this study are listed in Table S1. Precultures were grown in 2 ml
373 of LB Lennox medium (pH 7.3) at 37°C with shaking at 150 rpm overnight. Experimental
374 cultures were inoculated at a 1:100 ratio from precultures into LB Lennox and grown for 2.5
375 hours to reach the exponential phase (O.D. 600 = 0.4-0.5). Antibiotic treatments included
376 Polymyxin B (Pmb) at concentrations ranging from 0.5 µg/ml (0.25×MIC) to 2 µg/ml (1×MIC),
377 Colistin at 0.75 µg/ml (0.25×MIC) to 3 µg/ml (1×MIC), Tobramycin (tobra) at 0,1 µg/ml
378 (0.25×MIC) to 0.4 µg/ml (1×MIC) and Ciprofloxacin (Cip) at 10 ng/ml (0.2×MIC) to 50 ng/ml
379 (1×MIC). Fluorescent polymyxin B (Rhodamine-Pmb) was used at concentrations from 1.5
380 µg/ml (0.18×MIC) to 8 µg/ml (1×MIC). Unless otherwise noted, bulk experiments were
381 conducted with Pmb and Pmb_{fl} at 0.5×MIC. All antibiotics were purchased at Sigma Aldrich.

382

383 **EV production, isolation and purification**

384 A 1:100 dilution of an overnight culture of wild-type (wt) bacteria (or *ompA* mutants when
385 noted, for increased EV production yields due to their hyper-vesiculation phenotype) was used
386 to inoculate 50 ml of fresh LB medium. Cultures were grown for 1, 2, 4, 6.5 or 20 hours, with
387 or without Pmb antibiotic, and cells were removed by centrifugation (5000 rpm, 10°C, 30 min;
388 Eppendorf 5810 R centrifuge). The EV isolation protocol was adapted from previous study⁴⁸.
389 EVs were purified through filtration and ultracentrifugation. The supernatants were filtered
390 through a 0.22 µm unit with a 50 ml syringe. To ensure the absence of bacterial contamination,
391 150 µl of the filtrate was plated onto LB agar and incubated at 37°C overnight; no colonies
392 were observed after 24-48 hours. EVs were pelleted by ultracentrifugation at 41,000 rpm for
393 3 hours at 4°C (Optima L-80 XP ultracentrifuge, Beckman Coulter) using a 45Ti rotor.

394 Supernatants were carefully and completely removed and EV pellets were resuspended in 0.5
395 ml of freshly filtered phosphate-buffered saline (PBS; EDTA- and CaCl₂-free, pH 7.5, 1×,
396 filtered through 0.1 μm units), yielding a 100-fold concentration. Samples were stored at 4°C
397 for no longer than one week and validated for EV presence using fluorescence microscopy
398 and cryo-electron microscopy (Figure S9). We showed that the origin of EVs (had a negligible
399 impact in our assays (Figure S2) therefore for most experiments, we used EVs purified from
400 *ompA* cells unless noted as the yield of production was increased by about 100 times.
401 Absolute EV concentrations and size distributions were determined using a nano-flow
402 cytometer (NanoFCM Technology) (Figure S9) at the Flow Cytometry facility, CR2T, Institut
403 Pasteur. Means of concentrations of pure EV samples used in the study are reported in Table
404 S2; They ranged from 1.2 10⁺¹⁰ EVs/ml (wt donor), 2.5 10⁺¹¹ EVs/ml (*ompA* donor) and 1.4
405 10⁺¹¹ EVs/ml (wt + Pmb donor). For EV uptake assays, filtered supernatants of *ompA* cell
406 cultures were stained at 37°C for 20 minutes with lipophilic dyes (FM1-43 (green) and FM4-
407 64 (red)) at a final concentration of 0.6 mg/ml. EVs were then pelleted by ultracentrifugation
408 using the same protocol described above.

409

410 **Growth curves assays**

411 We used a TECAN Infinite 200 PRO microplate reader for automated measurement of
412 population growth curves with or without antibiotic stress, quantification of membrane-stress
413 reporter expression (*rcaA-gfp*), quantification of Pmb_{fl} decay (insertion of Pmb_{fl} in cell
414 membranes and EVs). Bacterial growth curves experiments were conducted over 800 minutes
415 unless noted with fluorescence reads at 474 nm (*rcaA-gfp*,) or 560 nm (Pmb_{fl}) when needed.
416 Wells were inoculated with 2.5 μl of precultures into 150 μl of LB medium, supplemented as
417 needed with antibiotics and/or EVs (~1.2 E+09; ~160 EV/cell) added concomitantly or with a
418 delay (30, 60 or 120 minutes) to the wells. Data were analyzed using GraphPad Prism 10.0.0
419 software (San Diego, California, USA)

420

421 **Whole genome sequencing of adapted populations**

422 To verify the presence of mutations in the Pmb-adapted populations, whole genome
423 sequencing of bacteria cultured in wells containing, LB only, LB + EVs, and LB + Pmb (1×MIC)
424 + EVs (~1.2 10⁺⁹ added to the culture; ~160 EV/cell) was performed at the end of the growth
425 curve run. Whole genome sequencing (WGS) was performed by the in-house Mutualized
426 Platform for Microbiology (Paris, France) using the Nextera XT DNA Library Preparation kit
427 (Illumina Inc.), the NextSeq 500 sequencing system (Illumina Inc.) and the CLC Genomics
428 Workbench 11 software (Qiagen) for analysis. Coverage of at least 50 X was obtained,
429 guaranteeing a good quality sequence. No mutations (SNPs or genetic rearrangements) were
430 identified using the following tools Breseq Variant Report - v0.35. for the cells cultured with
431 EVs, with and without Pmb.

432

433 **Time course of Pmb_{fl} dynamics and decay assays**

434 For the time course assay following Pmb_{fl} addition, we used 30 ml cultures (dilution 1:100 of
435 precultures) grown in fresh LB to exponential phase (~2.5 h). Before Pmb_{fl} addition, a 1.5 ml
436 sample (t=0) was harvested and O.D was measured. Then the sample was centrifuged (10K
437 rpm, 3 minutes), with the cell pellet immediately resuspended in PBS 1X (1.5 ml), and the
438 spent medium containing vesicles collected by 0.22 μm filtration. Further samples were

439 collected over time following the same protocol. All samples were imaged under the
440 microscope. For each sample, equal volumes of supernatant and cell pellet fractions were
441 distributed in six replicates into a 96-well black flat-bottom plate, and OD 600nm and total
442 fluorescence were measured at 560 nm using a TECAN Infinite M200 PRO microplate reader.
443 All samples were imaged under the microscope, on agar pads. For the time course assay
444 following Pmb_{fl} removal (decay assay), we used 10 ml cultures (dilution 1:100 of precultures)
445 grown in fresh LB to exponential phase (~2.0 h) then Pmb_{fl} was added for 30 minutes. Before
446 Pmb_{fl} removal a 1.5 ml sample (t=0) was harvested and the O.D measured. The rest of the
447 culture was centrifuged and the pellet was resuspended in fresh LB. Red fluorescence signal
448 and cell density were read at 560 nm and 600 nm respectively using a TECAN Infinite M200
449 PRO microplate reader. Samples were collected over time for microscopy imaging. In all
450 analyses, the fluorescence signal was normalized to cell density. Data were analyzed using
451 GraphPad Prism 10.0.0 software (San Diego, California, USA)

452

453 **Fluorescence microscopy imaging setup for bacterial cells, Pmb_{fl} and EV_{fluo}**

454 For all experiments, cell cultures were grown with or without sub-MIC antibiotics in liquid LB
455 medium to mid-exponential phase, then transferred to 1.3% agarose-padded slides containing
456 LB. A coverslip was placed on the agarose pad and sealed with a 1:1:1 mix of vaseline, lanolin,
457 and paraffin to prevent evaporation. Imaging was performed immediately at 37°C using a Zeiss
458 ApoTome inverted wide-field microscope for time-lapse analysis.

459 To study the interactions between Pmb, EVs, and bacteria, the antibiotic Rhodamine B-labeled
460 polymyxin B (Pmb_{fl}) was used. Snapshot images were captured at intervals of 0, 30, 60, 120
461 and 240 minutes after adding Pmb_{fl} (0.5×MIC) to cultures. Images were taken with a Plan Apo
462 63× objective (NA = 1.4, +optovar 1.6×) and recorded using a Hamamatsu ORCA-Flash 4.0
463 v3 sCMOS camera (Institut Pasteur Imaging Facility, CR2T).

464 Pmb_{fl} stained fractions (cell pellet and supernatant) were imaged using two channels: red (560
465 nm) and phase contrast. Fluorescent EVs were imaged in the red channel (560 nm) when
466 stained with the lipophilic dye FM4-64 (T3166, Thermo Fisher Scientific). EVs labeled with
467 FM1-43 (T3163, Thermo Fisher Scientific) and stressed bacteria (*rcaA-gfp*) were imaged in
468 the green channel (FITC, 488 nm). Images were analyzed using FIJI software⁴⁹ or MicrobeJ
469 image analysis software⁵⁰

470

471 **Sample preparation for EV uptake analysis**

472 Wild-type (wt), wt pPrcaA-*gfp*, and *ompA* cells were grown in 20 ml of LB Lennox medium at
473 37°C for 2.5 hours from 1:100 diluted precultures. A 0.5 ml aliquot of culture (10⁺⁸ cells) was
474 transferred into 2 ml Eppendorf tubes. When required, antibiotics (polymyxin B (Pmb, 0.5×MIC
475 final), fluorescent Pmb (Pmb_{fl}, 0.5×MIC final), ciprofloxacin (0.4×MIC final), or colistin
476 (0.5×MIC final)) and EVs (10 μl of pure fraction at 10⁺¹⁰ particles/ml, stained or unstained)
477 were added to the 0,5 ml culture tubes. Tubes were incubated at 37°C with shaking for 30
478 minutes (tubes lay down with tape). For EV uptake experiments, fluorescently labeled EVs
479 (~1×10⁺¹⁰ EVs (native) or EVs (Pmb-loaded); mean ratio of 72 EV/cell, Table S2) were added
480 for 10 minutes immediately after antibiotic exposure (30 minutes) and the culture mix was put
481 at 37°C with shaking. Then the samples were centrifuged at 13,000 rpm for 4 minutes,
482 supernatants were carefully discarded to remove the drug and the EVs, and the cell pellets
483 were resuspended in 0.5 ml of filtered 1×PBS (100 nm filter, FischerBrand). Tubes were

484 wrapped with foil before further analysis. Samples were imaged using a Zeiss ApoTome
485 inverted wide-field microscope (UtechS Photonic Biolmaging (Imagopole)) for controls.

486

487 **Flow cytometry and cell sorting workflow**

488 For flow cytometry, samples were diluted 1:10 and analyzed with a CytoFLEX flow cytometer
489 S (Beckman Coulter, France), operated with the CytExpert software (Beckman Coulter,
490 France). The machine is equipped with 488 nm (50 mW), 561 nm (30 mW) lasers. The 488
491 nm laser light was used for the detection of forward scatter (FSC) (488/8 nm band-pass), side
492 scatter (SSC) (488/8 nm band-pass) a double threshold on both parameters. The FITC
493 fluorescence (525/40 nm band-pass) was measured using the 488 nm laser for excitation and
494 PE (585/42/80 nm band pass) was measured using the 561 nm laser. The fluidic system ran
495 at a constant speed of 30 $\mu\text{L}/\text{min}$. Fluorescence intensity and cell counts (N=50000 for each
496 sample) were measured using an automated method for diluted live bacterial cells.

497 Cell Sorting was performed with the MoFlo Astrios (Beckman Coulter, France) at 25 PSI with
498 a 100 nM nozzle at approximately 6000 events per second. The FSC and SSC were read
499 logarithmically with the 488 laser. FITC fluorescence was read with the 488 laser (576/21 band
500 pass) and PE (579/16 band pass) with 561 laser. Samples treated with Pmb and
501 supplemented with fluorescent EVs were sorted and analyzed. Sorted populations (various
502 cell counts, 5000-25000 cells) included unstained cells, red (PE, EV-patched), green (FITC,
503 *rcsA-gfp*⁺ stressed), and red+green (EV-patched *rcsA-gfp*⁺ stressed) cells. All data were
504 processed using Flowjo software FlowJo v10.10.0, Becton, Dickinson and Company, Ashland,
505 Oregon, USA. For growth recovery experiment, cell counts were normalized across sorted
506 populations when seeding the wells of the 96-well plate. Data were analyzed using GraphPad
507 Prism 10.0.0 software (San Diego, California, USA). For all experiments, representative
508 histograms (FSC, FITC or PE intensity) are available in the *Supplemental material*.

509

510 **Cryo-electron Tomography**

511 For *sample preparation*, an overnight culture (1 ml) was centrifuged, and the pellet was
512 resuspended in 0.6 ml of fresh LB, with or without Polymyxin B (0.5 \times MIC) and 0.1 ml of pure
513 EVs. The tubes were incubated at 37°C for 90 minutes, centrifuged to remove excess EVs
514 and drug, and then resuspended in 1 \times PBS. A 4 μl volume of the sample mix was drop casted
515 on glow discharged Quantifoil R 2/2 on 200 gold mesh grids (Oxford/Quantifoil) and left to
516 adsorb for 1 minute. Cell density on the grid was then verified using an upright Zeiss Apotome
517 microscope (brightfield channel) before the back blotting step against Whatman paper for 7
518 seconds. Cryo-fixation performed by plunge freezing at -180 °C 75% humidity in liquid ethane
519 using a Leica EMGP (Leica, Austria). The grids were then immediately transferred for storage
520 in liquid Nitrogen before data collection.

521 Regarding the imaging protocol and equipment, dose-symmetric tilt series were collected on
522 a 300 kV Titan Krios (Thermo Scientific) transmission electron microscope equipped with
523 Falcon 4i direct electron detector (Thermo Scientific) and Selectris X imaging filter (Thermo
524 Scientific). Tomography software (Thermo Scientific) was used to acquire tilt series with a tilt
525 span of $\pm 45^\circ$ and an angular increment of 3° . The total electron dose was approx. 120
526 electrons per \AA^2 and the pixel size at 3.101 \AA . Tilt series were saved as separate stacks of
527 .eer frames and subsequently motion-corrected and coarse aligned using IMOD software. In
528 parallel with data collection, an on-the-fly reconstruction software Tomo Life (Thermo

529 Scientific) was used to both judge the quality of acquired data and reconstruction. Further,
530 aligned stacks were de-noised using IsoNet for better visualization.

531 **Acknowledgments** - We thank all the Mazel lab members for their helpful discussion, Morgan
532 Lamberieux for his help with sequencing data, Anna Sartori-Rupp (NICF) and Stéphane
533 Tachon (NICF) for their guidance with Cryo-EM. We also thank JM Ghigo's lab for its kind gift
534 of strains. We gratefully acknowledge the Flow Cytometry platform, the Nanoimaging core
535 facility, the UtechS Photonic Bioimaging facility (Imagopole, C2RT, supported by the French
536 National Research Agency (France Bioimaging; ANR-10-INBS-04; Investments for the
537 Future) at Institut Pasteur for support in conducting this study. We also thank the platform
538 "microbiologie mutualisée (P2M), Pasteur International Bioresources Network (PIBnet)" at
539 Institut Pasteur for support in genome sequencing service. We acknowledge the use of AI-
540 based writing tools (ChatGPT) for language enhancement.

541 **Author contribution:** D.M supervised the research. J.B conceived the research. J.B, Y.AH,
542 PH.C and O.M performed the experiments. J.B and D.M funded the research. J.B wrote the
543 the manuscript. All authors read and approved the final manuscript.

544 **Fundings:** This work was supported by the Institut Pasteur, the Centre National de la
545 Recherche Scientifique (CNRS-UMR 3525), the Fondation pour la Recherche Médicale Grant
546 No.EQU202103012569, the French Government's Investissement d'Avenir program
547 Laboratoire d'Excellence "Integrative Biology of Emerging Infectious Diseases" Grant
548 No. ANR-10-LABX-62-IBEID and by the ANR MicroVesi ANR-22-CE35-0014-01.

549
550 **Conflict of interest:** None declared

551 552 **References**

- 554 1. Naghavi, M. *et al.* Global burden of bacterial antimicrobial resistance 1990–2021: a
555 systematic analysis with forecasts to 2050. *The Lancet* 1–28 (2024)
556 doi:10.1016/S0140-6736(24)01867-1.
- 557 2. Poirel, L., Jayol, A. & Nordmanna, P. Polymyxins: Antibacterial activity, susceptibility
558 testing, and resistance mechanisms encoded by plasmids or chromosomes. *Clin*
559 *Microbiol Rev* 30, 557–596 (2017).
- 560 3. Falagas, M. E. & Kasiakou, S. K. Toxicity of polymyxins: A systematic review of the
561 evidence from old and recent studies. *Crit Care* 10, (2006).
- 562 4. De Fátima Fernandes Vattimo, M. *et al.* Polymyxin B Nephrotoxicity: From organ to
563 cell damage. *PLoS One* 11, 1–17 (2016).
- 564 5. BENEDICT RG, L. AF. Antibiotic activity of Bacillus polymyxa. *J Bacteriol* 54, (1947).
- 565 6. Guaní-Guerra, E., Santos-Mendoza, T., Lugo-Reyes, S. O. & Terán, L. M.
566 Antimicrobial peptides: General overview and clinical implications in human health
567 and disease. *Clinical Immunology* 135, 1–11 (2010).
- 568 7. Trimble, M. J., Mlynářčík, P., Kolář, M. & Hancock, R. E. W. Polymyxin: Alternative
569 mechanisms of action and resistance. *Cold Spring Harb Perspect Med* 6, 1–22
570 (2016).
- 571 8. Padhy, I., Dwibedy, S. K. & Mohapatra, S. S. A molecular overview of the polymyxin-
572 LPS interaction in the context of its mode of action and resistance development.
573 *Microbiol Res* 283, 127679 (2024).

- 574 9. Mohapatra, S. S., Dwibedy, S. K. & Padhy, I. Polymyxins, the last-resort antibiotics:
575 Mode of action, resistance emergence, and potential solutions. *J Biosci* 46, (2021).
- 576 10. Liu, Y. Y. *et al.* Emergence of plasmid-mediated colistin resistance mechanism MCR-
577 1 in animals and human beings in China: A microbiological and molecular biological
578 study. *Lancet Infect Dis* 16, 161–168 (2016).
- 579 11. Buchholz, K. R. *et al.* Potent activity of polymyxin B is associated with long-lived
580 super-stoichiometric accumulation mediated by weak-affinity binding to lipid A. *Nat*
581 *Commun* 15, (2024).
- 582 12. Deris, Z. Z. *et al.* Probing the penetration of antimicrobial polymyxin lipopeptides into
583 gram-negative bacteria. *Bioconjug Chem* 25, 750–760 (2014).
- 584 13. Ernst T. Rietschel, Teruo Kirikae, F. Ulrich Schade, Uwe Mamat, Günter Schmidt,
585 Harald Loppnow, Artur J. Ulmer, Ulrich Zähringer, Ulrich Seydel, Franco Di Padova,
586 Max Schreier, H. B. Bacterial endotoxin: molecular relationships of structure to activity
587 and function. *FASEB* (1994).
- 588 14. Fu, L., Wan, M., Zhang, S., Gao, L. & Fang, W. Polymyxin B Loosens
589 Lipopolysaccharide Bilayer but Stiffens Phospholipid Bilayer. *Biophys J* 118, 138–150
590 (2020).
- 591 15. Oh, Y. J., Plochberger, B., Rechberger, M. & Hinterdorfer, P. Characterizing the effect
592 of polymyxin B antibiotics to lipopolysaccharide on Escherichia coli surface using
593 atomic force microscopy. *Journal of Molecular Recognition* 30, 1–7 (2017).
- 594 16. Manning, A. J. *et al.* Characterizing the effect of polymyxin B antibiotics to
595 lipopolysaccharide on Escherichia coli surface using atomic force microscopy. *Nat*
596 *Commun* 15, 1–7 (2024).
- 597 17. Manioglu, S. *et al.* Antibiotic polymyxin arranges lipopolysaccharide into crystalline
598 structures to solidify the bacterial membrane. *Nat Commun* 13, (2022).
- 599 18. Vaara, M. & Viljanen, P. Binding of polymyxin B nonapeptide to gram-negative
600 bacteria. *Antimicrob Agents Chemother* 27, 548–554 (1985).
- 601 19. Mitchell, A. M. & Silhavy, T. J. Envelope stress responses: balancing damage repair
602 and toxicity. *Nat Rev Microbiol* 17, 417–428 (2019).
- 603 20. Danese, P. N. & Silhavy, T. J. The $\sigma(E)$ and the Cpx signal transduction systems
604 control the synthesis of periplasmic protein-folding enzymes in Escherichia coli.
605 *Genes Dev* 11, 1183–1193 (1997).
- 606 21. Stout, V. & Gottesman, S. RcsB and RcsC: A two-component regulator of capsule
607 synthesis in Escherichia coli. *J Bacteriol* 172, 659–669 (1990).
- 608 22. Li, Z., Zhu, Y., Zhang, W. & Mu, W. Rcs signal transduction system in Escherichia
609 coli: Composition, related functions, regulatory mechanism, and applications.
610 *Microbiol Res* 285, 127783 (2024).
- 611 23. Laubacher, M. E. & Ades, S. E. The Rcs phosphorelay is a cell envelope stress
612 response activated by peptidoglycan stress and contributes to intrinsic antibiotic
613 resistance. *J Bacteriol* 190, 2065–2074 (2008).
- 614 24. Nadim Majdalani¹, and S. G. THE RCS PHOSPHORELAY: A Complex Signal
615 Transduction System. *Annu Rev Microbiol* 59, (2005).
- 616 25. Bader, M. W. *et al.* Recognition of antimicrobial peptides by a bacterial sensor kinase.
617 *Cell* 122, 461–472 (2005).
- 618 26. Kox, L. F. F., Wösten, M. M. S. M. & Groisman, E. A. A small protein that mediates
619 the activation of a two-component system by another two-component system. *EMBO*
620 *Journal* 19, 1861–1872 (2000).
- 621 27. Winfield, M. D. & Groisman, E. A. Phenotypic differences between Salmonella and
622 Escherichia coli resulting from the disparate regulation of homologous genes. *Proc*
623 *Natl Acad Sci U S A* 101, 17162–17167 (2004).
- 624 28. MacNair, C. R. & Tan, M. W. The role of bacterial membrane vesicles in antibiotic
625 resistance. *Ann N Y Acad Sci* 1519, 63–73 (2023).

- 626 29. Manning, A. J. & Kuehn, M. J. Contribution of bacterial outer membrane vesicles to
627 innate bacterial defense. *BMC Microbiol* 11, (2011).
- 628 30. Park, J. *et al.* A novel decoy strategy for polymyxin resistance in acinetobacter
629 baumannii. *Elife* 10, 1–29 (2021).
- 630 31. Kulkarni, H. M., Nagaraj, R. & Jagannadham, M. V. Protective role of E. coli outer
631 membrane vesicles against antibiotics. *Microbiol Res* 181, 1–7 (2015).
- 632 32. Kulkarni, H. M., Swamy, C. V. B. & Jagannadham, M. V. Molecular characterization
633 and functional analysis of outer membrane vesicles from the Antarctic bacterium
634 Pseudomonas syringae suggest a possible response to environmental conditions. *J*
635 *Proteome Res* 13, 1345–1358 (2014).
- 636 33. Marchant, P. *et al.* β -lactam-induced OMV release promotes polymyxin tolerance in
637 Salmonella enterica sv. Typhi. *Front Microbiol* 15, (2024).
- 638 34. Chen, Z. *et al.* Bacterial outer membrane vesicles increase polymyxin resistance in
639 Pseudomonas aeruginosa while inhibiting its quorum sensing. *J Hazard Mater* 478,
640 135588 (2024).
- 641 35. Marchant, P. *et al.* “One for All”: Functional Transfer of OMV-Mediated Polymyxin B
642 Resistance From Salmonella enterica sv. Typhi Δ tolR and Δ degS to Susceptible
643 Bacteria. *Front Microbiol* 12, (2021).
- 644 36. Kim, S. W. *et al.* Outer membrane vesicles from β -lactam-resistant Escherichia coli
645 enable the survival of β -lactam-susceptible E. coli in the presence of β -lactam
646 antibiotics. *Sci Rep* 8, (2018).
- 647 37. Stanton, A. E. & Hughson, F. M. The machinery of vesicle fusion. *Curr Opin Cell Biol*
648 83, 102191 (2023).
- 649 38. Söllner, T. *et al.* Targeting and Fusion. 362, (1993).
- 650 39. Rothman, J. E. Mechanisms of Intracellular Protein Transport. *Biol Chem Hoppe*
651 *Seyler* 377, 407–410 (1996).
- 652 40. Hurley, J. H. & Hanson, P. I. Membrane budding and scission by the ESCRT
653 machinery: It’s all in the neck. *Nat Rev Mol Cell Biol* 11, 556–566 (2010).
- 654 41. Junglas, B. *et al.* PspA adopts an ESCRT-III-like fold and remodels bacterial
655 membranes. *Cell* 184, 3674–3688.e18 (2021).
- 656 42. Kulp, A. & Kuehn, M. J. Biological Functions and biogenesis of secreted bacterial
657 outer membrane vesicles. *Annual Review of Microbiology* vol. 64 163–184 Preprint at
658 <https://doi.org/10.1146/annurev.micro.091208.073413> (2010).
- 659 43. Gamazo, C. & Moriyon, I. Release of outer membrane fragments by exponentially
660 growing Brucella melitensis cells. *Infect Immun* 55, 609–615 (1987).
- 661 44. Hoekstra, D., van der Laan, J. W., de Leij, L. & Witholt, B. Release of outer
662 membrane fragments from normally growing Escherichia coli. *BBA - Biomembranes*
663 455, 889–899 (1976).
- 664 45. McBroom, A. J. & Kuehn, M. J. Release of outer membrane vesicles by Gram-
665 negative bacteria is a novel envelope stress response. *Mol Microbiol* 63, 545–558
666 (2007).
- 667 46. Bos, J., Cisneros, L. H. & Mazel, D. Real-time tracking of bacterial membrane vesicles
668 reveals enhanced membrane traffic upon antibiotic exposure. *Sci Adv* 7, 1–11 (2021).
- 669 47. Schindelin, J. *et al.* Fiji: An open-source platform for biological-image analysis. *Nat*
670 *Methods* 9, 676–682 (2012).
- 671 48. Ducret, A., Quardokus, E. M. & Brun, Y. V. MicrobeJ, a tool for high throughput
672 bacterial cell detection and quantitative analysis. *Nat Microbiol* 1, 1–7 (2016).

673

674

675 **Figures**

676

677

678

679

680

681

682

683

684

685

686

687

688

689

690

691

692

693

694

695

696

697

698

699

700

701

702

703

704

705

706

707

708

709

710

711

712

713

714

715

716

717

718

719

720

721

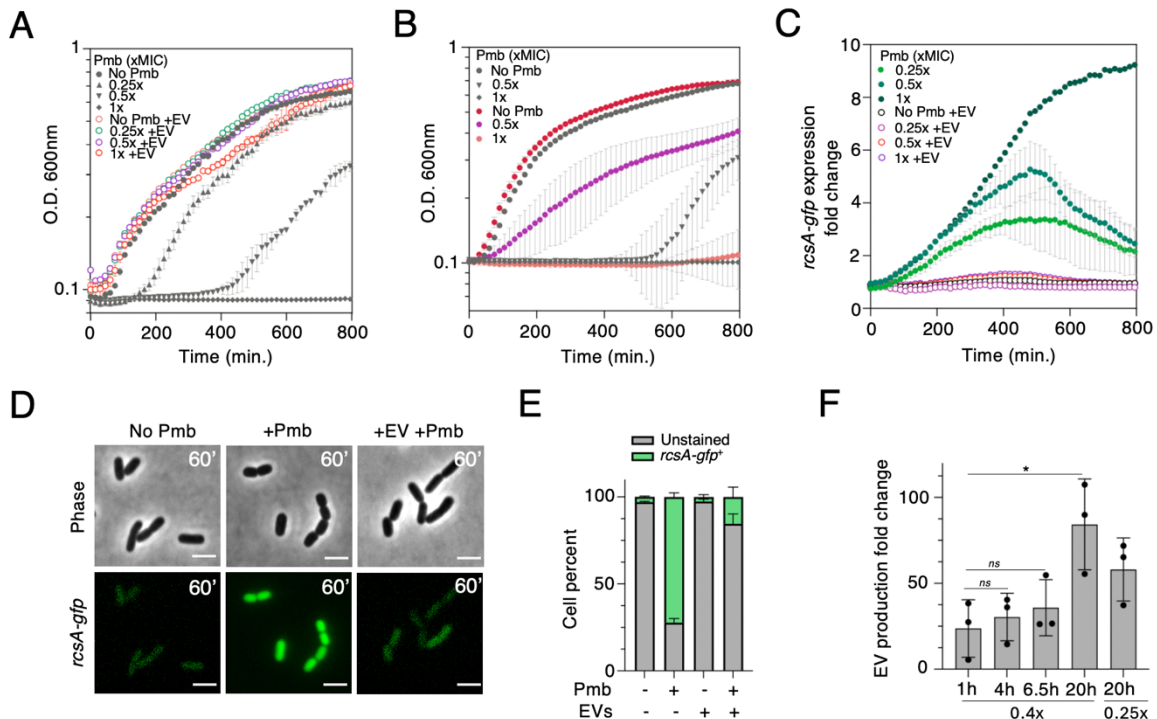


Figure 1: Sub-MIC Polymyxin B triggers RcsA-mediated stress response, enhanced

vesicle production, and adaptive population tolerance in *E. coli*.

A. Growth curves of wild type (wt) *E. coli* in the absence or presence of various doses of Pmb (0.25x, 0.5x, and 1x MIC; dark grey) with or without the concomitant addition of pure EVs (empty circles). **B.** Growth curves of naïve and adapted cells with or without various doses of Pmb (0.5x and 1xMIC). Naïve cells (dark grey) have never been exposed to Pmb while adapted cells (colored circles) are wt cells previously grown with Pmb 0.5x and in the presence of pure EVs. **C.** sub-MIC Pmb induces expression of pPr*r*csA-*gfp*, a marker for envelop stress. The effect of various Pmb doses (0.25x, 0.5x, 1xMIC; green circles) and the effect of concomitant EV addition (empty circles) on pPr*r*csA-*gfp* expression levels are shown. All growth curves were obtained from three independent biological samples. **D.** Microscopy snapshots of wt cells carrying pPr*r*csA-*gfp* under exposure to Pmb (0.5xMIC), with and without EVs, at 60 min following Pmb addition, illustrating quantification in D. Phase contrast and FITC (*r*csA-*gfp*) images are shown. Scale bar is 2 microns. **E.** Single-cell quantification (flow cytometry) showing the percentage of cells expressing *r*csA-*gfp*, with and without EVs, at 60 minutes following Pmb addition (0.5x MIC). N = 50,000 represents the total number of cells counted in each biological replicate (n=3). **F.** Quantification of EV production (Fold change compared to “no Pmb” condition) after 1, 2, 4, 6.5 and 20 hours of growth with sub-MIC Pmb (0.4x MIC, or 0.25x MIC at t=20h) using nano-flow cytometry. Statistical significance (unpaired t-test) is indicated (ns, not significant, * $P=0.04$). In all plots, error bars represent standard deviation.

722
723
724
725
726
727
728
729
730
731
732
733
734
735
736
737
738
739
740
741
742
743
744
745
746
747
748
749
750
751
752
753
754
755
756
757
758
759
760
761
762
763
764
765
766
767
768

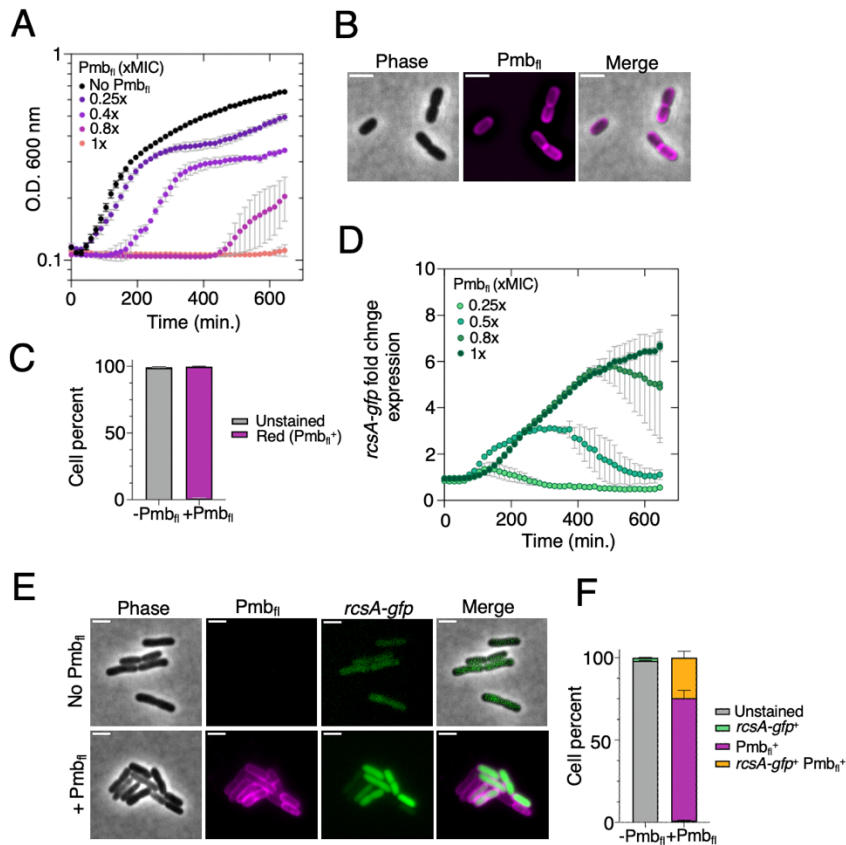


Figure 2: Pmb_{fl} fluorescent antibiotic decorates *E. coli* outer membranes and triggers membrane stress response. A. Growth curves of wt bacteria in the absence or presence of various concentrations of Pmb_{fl}. B. Microscopy images showing Pmb_{fl} insertion into cell membranes. Phase contrast, TRITC (red; Pmb_{fl}⁺), and merged images are displayed. C. Single-cell quantification (flow cytometry) of Pmb_{fl} insertion efficiency in wt bacteria. The drug was added for 30 min at a concentration of 0.5x MIC. D. Expression levels of membrane stress response over time, as a function of various Pmb_{fl} concentrations. Expression fold change varies from 3x (0.4x Pmb_{fl}) to 7x (1x Pmb_{fl}). All growth curves were obtained from three independent biological samples. E. Microscopy images of wt cells carrying pPr*rscA-gfp* (kan) cultured to exponential phase and treated with or without 0.5x MIC Pmb_{fl} for 30 min. Phase contrast, fluorescent images in the TRITC channel (Pmb_{fl}) and FITC channel (*rscA-gfp*) along and merged images are shown. F. Single-cell quantification plot (flow cytometry, n=2) showing the percentage of cells expressing *rscA-gfp* (green⁺ only), decorated with Pmb_{fl} (red⁺ only), *rscA-gfp* stressed cells decorated with Pmb_{fl} (red⁺ and green⁺) and not fluorescent (unstained) cells after 30 min of exposure to 0.5x MIC Pmb_{fl} or in the absence of Pmb_{fl}.

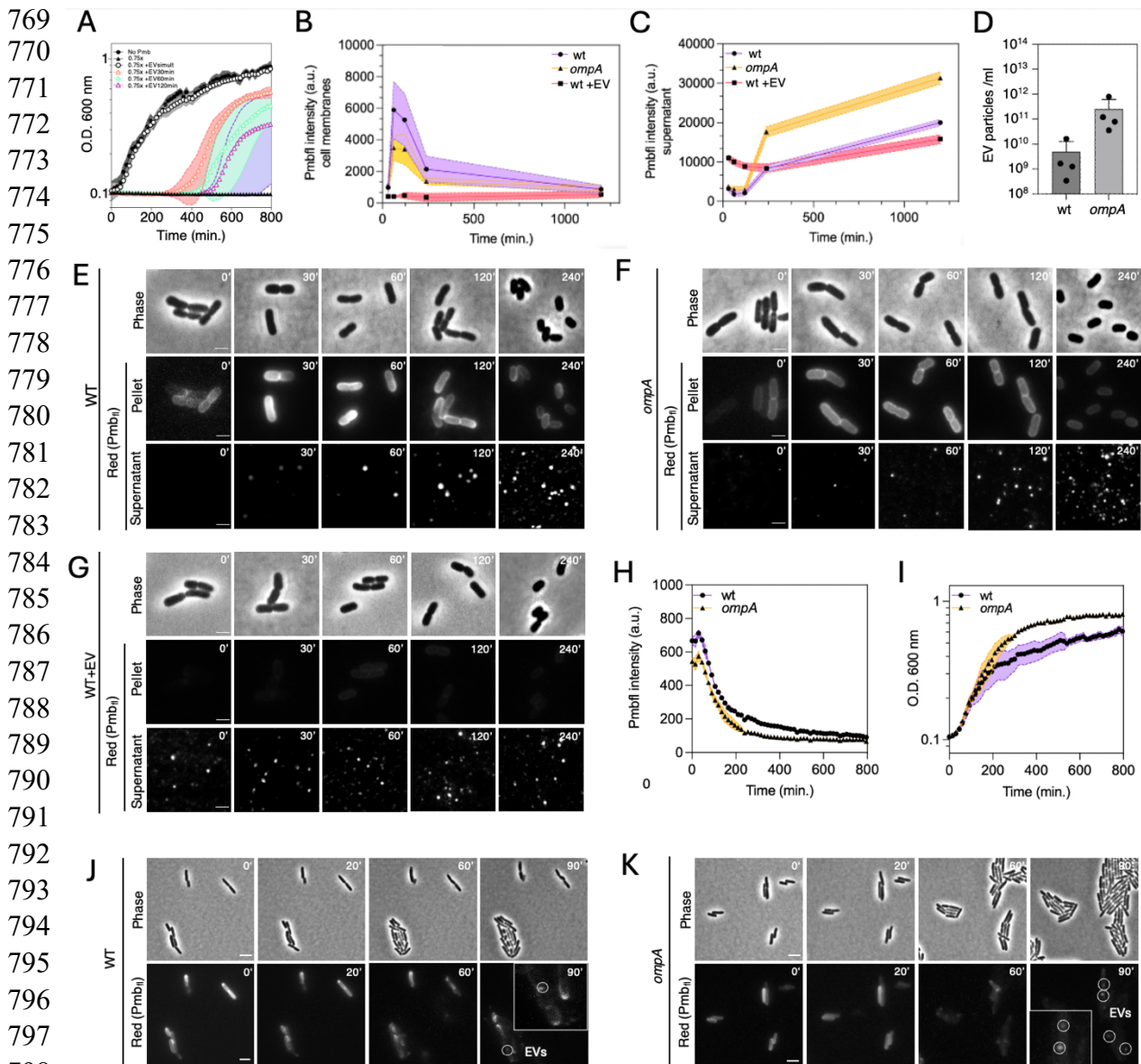


Figure 3: Vesiculation aids in trapping and clearing Pmb antibiotic from cell membranes. A. Growth curve assay of wt strain with delayed (30, 60, 120 min; empty triangles) or simultaneous (0 min, empty circle) addition of pure EVs with Pmb (0.75x MIC). Standard deviations are represented by the shaded areas, calculated from six independent experiments. B-C. Quantification of Pmb_{fl} fluorescence signal in cell membranes (pellets) (B) and cell culture supernatants after filtration (C) during a time course assay. Cells (wt, *ompA*, wt + pure EVs) were exposed to Pmb_{fl} for 0, 30, 60-, 120-, 240- and 1200-minutes. Fluorescence signal is normalized to cell density (OD 600 nm). Standard deviation is indicated (n= 3 independent experiments). D. EV production counts (particle/ml) in wt cells compared to hypervesiculating *ompA* mutant cells, which release higher endogenous EV loads (~20x more). Standard deviation is indicated, calculated from 4 independent experiments. E-F-G. Fluorescence microscopy time course images of Pmb_{fl} insertion into cell membranes and EV particles present in the supernatant, for all tested conditions (wt, *ompA*, wt + pure EVs). Phase contrast and TRITC (red; Pmb_{fl}⁺) images are shown. Pmb_{fl} insertion in the cell membranes appears as discrete fluorescent cell contours, while insertion in EVs is shown as bright white dots in the supernatant. Scale bar is 2 microns. H. Pmb_{fl} fluorescent signal decay in cell

815 membranes of both wt and *ompA* cell populations, following Pmb_{fl} removal (t=0). Cells were
816 cultured in 96 well plates over 800 min. Standard deviation is indicated, based on three
817 independent experiments. I. Cell growth recovery of Pmb_{fl} (30 minutes) treated bacteria (wt
818 and *ompA*) following Pmb_{fl} removal (t=0). Standard deviation is indicated based on three
819 independent experiments. J-K. Microscopy time-course images showing Pmb_{fl} decay in single
820 cells (wt and *ompA*). Phase contrast and TRITC (red; Pmb_{fl}⁺) images are shown. After 90 min
821 of Pmb removal, microcolonies begin to form and EV-containing Pmb_{fl} (white circles and inlet)
822 start detaching from cell membranes. Scale bar is 2 microns. Movies of detached EVs
823 dispersing in a wt (Movie S1) and *ompA* (Movie S2) microcolony are available in the
824 supplementary information.

825
826
827
828
829
830
831
832
833
834
835
836
837
838
839
840
841
842
843
844
845
846
847
848
849
850
851
852
853
854
855
856
857
858
859
860
861
862
863

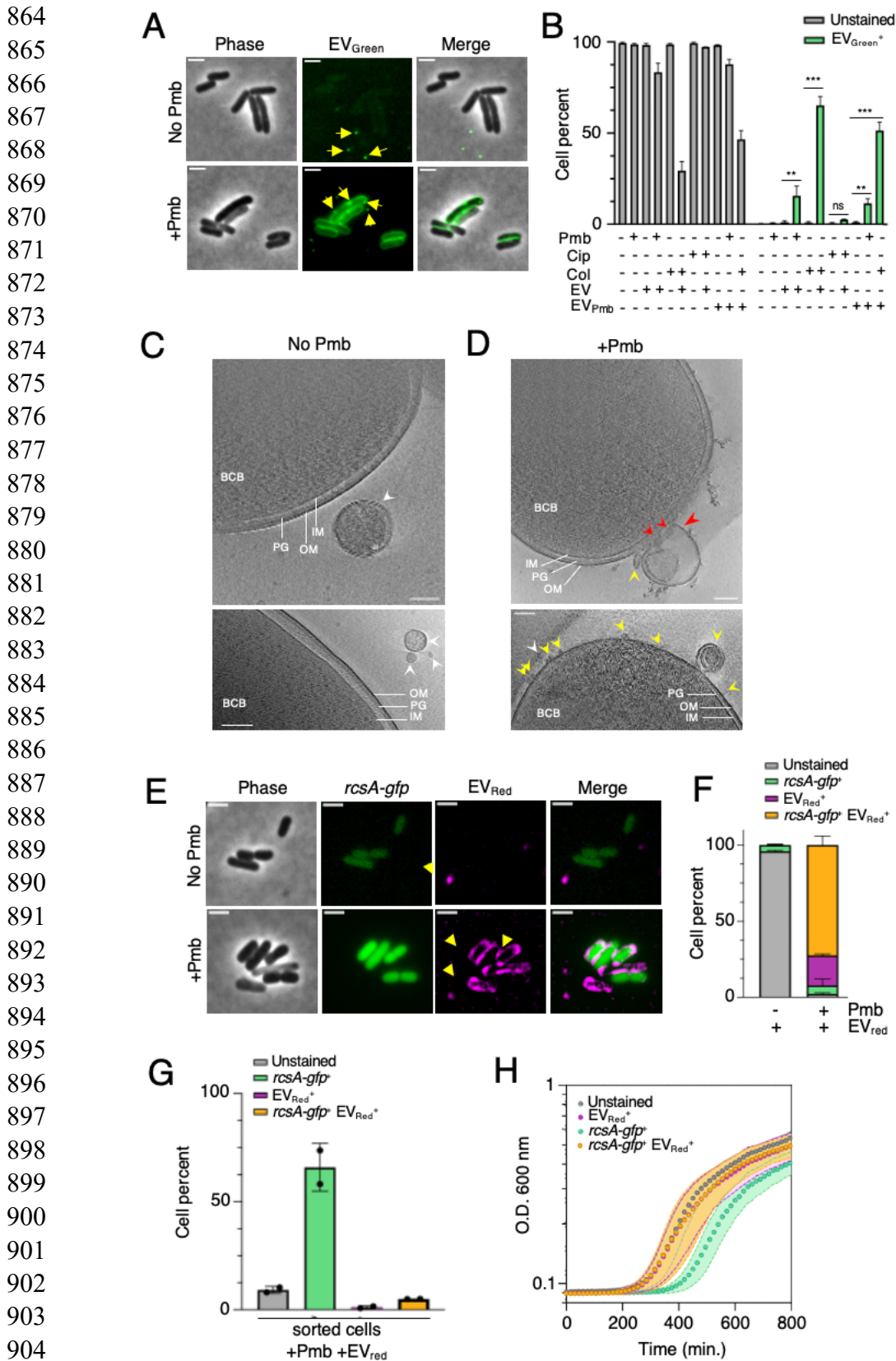


Figure 4: Uptake of fluorescently labeled EVs by *E. coli* membranes facilitates recovery of stressed bacteria. A. Microscopy images showing the uptake of fluorescent EVs (EV_{Green}) in wt cells either challenged with Pmb for 30 min., or left untreated. EVs were added for 10 min. after the initial 30 min. incubation time with or without Pmb, then removed by

910 centrifugation. Phase contrast and FITC channel images were captured. Scale bar is 2 μ m. B.
911 Quantification histogram of EV_{Green} and EV_{Pmb Green} (Pmb-loaded EVs) uptake in the presence
912 of various antibiotics (0.5x MIC), including membrane-active (Pmb and Colistin) and a non-
913 membrane targeting (Cip) antibiotic. Statistical significance is indicated (t-test) based on three
914 independent experiments (ns, 0.05<P<0.5; ** P \leq 0.01; *** P \leq 0.001). C-D. Cryo-electron
915 micrographs depicting EV interactions with *E. coli* cells, cultured in the absence of Pmb (No
916 Pmb) (C) or with Pmb antibiotic (0.5x MIC) for 60 min. (D). Pure EVs were added to the cell
917 mixture for 30 min. post-Pmb stress. The sample mixes were centrifuged and resuspended in
918 PBS to remove the majority of EVs (non-adherent to membranes) before plunge freezing. The
919 bacterial cell bodies (BCB) are indicated along with the outer (OM) and inner (IM) membranes
920 of the cell, the intermembrane peptidoglycan (PG) mesh, and the EVs in proximity to- (white
921 arrow), adhering (yellow arrow) or fused (red arrow) to the outer membrane. Scale bar is 100
922 nm in all images. E. Two-color fluorescence imaging of Pmb-stressed bacteria (wt pPrccsA-
923 *gfp*) and EV_{Red} uptake. Phase contrast, FITC, TRITC and merged FITC/TRITC channel images
924 are shown. Scale bar is 2 μ m. F. Single-cell analysis by flow cytometry of EV_{Red} uptake by
925 Pmb-stressed bacteria (wt pPrccsA-*gfp*) (n=3; standard deviation is indicated). G.
926 Quantification histogram of cell sorting assays (flow cytometry) showing the percentage of
927 sorted subpopulations of wt pPrccsA-*gfp* cells after 30 min. of 0.5x MIC Pmb exposure and 10
928 min. of EV_{Red} treatment. Cells were spun down to remove excess non-fused EVs and
929 resuspended in PBS before sorting (n=2; standard deviation is indicated). H. Growth curve
930 analysis of sorted cell subpopulations in the absence of Pmb. Standard deviation is indicated
931 based on two independent experiments with 6 replicates each.

932
933

934

935

936

937

938

939

940

941

942

943

944

945

946
947
948
949
950
951
952
953
954
955
956
957
958
959
960
961
962
963
964
965
966
967
968
969
970
971
972
973
974
975
976
977
978

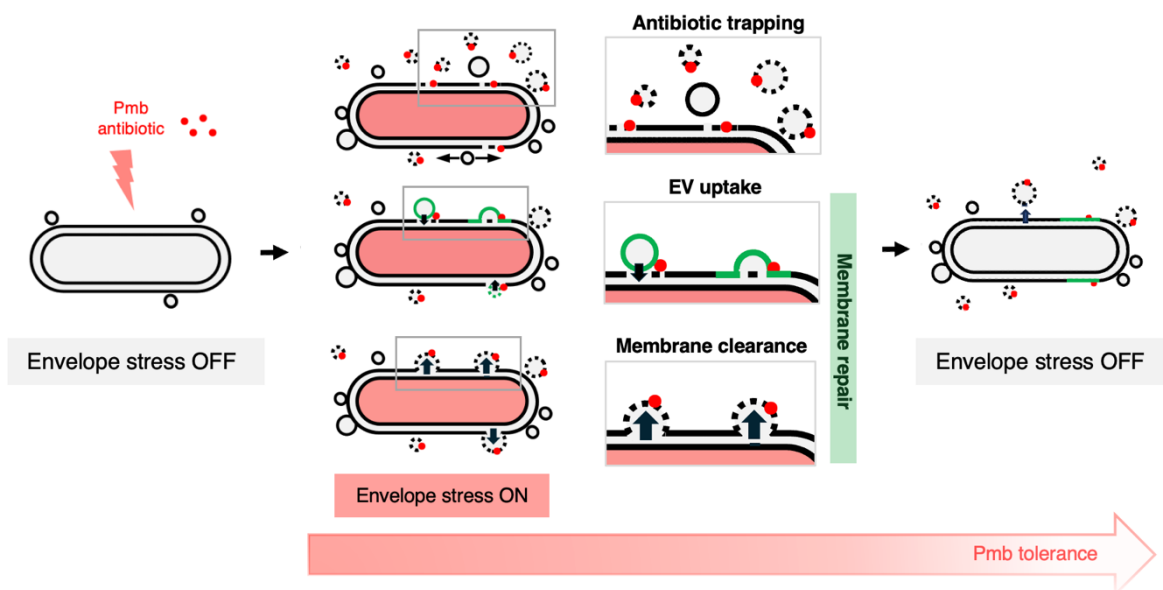


Figure 5: Working model illustrating the real-time interplay between extracellular vesicles (EVs), *E. coli* bacteria and Polymyxin B antibiotic. When *E. coli* is exposed to sub-MIC doses of Pmb (red dots), the bacteria shed EVs (black circles) near their membranes (black lines), triggering an RcsA-dependent envelope stress response (red). These EVs act as rapid traps for the Pmb antibiotic and contribute to membrane repair by removing the antibiotic and damaged areas from the membranes (dashed circles). Additionally, EVs loaded or not with Pmb (dashed green versus green circles respectively), can fuse with membranes, suggesting a role in patching damaged areas during stress. The role of Pmb-loaded EVs in uptake remains uncertain, but their smaller size could possibly facilitate intermembrane fusion. Stressed cells that are patched with EVs demonstrate improved growth recovery compared to non-patched cells. Thus, EVs play a critical role in managing membrane stress, deactivating the stress response, and enhancing bacterial tolerance to the antibiotic. Our single-cell assays highlight the dual roles of EVs in antibiotic trapping and membrane repair, shedding light on mechanisms that contribute to Pmb tolerance, a significant public health concern due to the increasing prevalence of Pmb-resistant microorganisms.

979 **Supplemental information of the manuscript “Extracellular vesicle production and**
980 **membrane uptake promote repair and antibiotic tolerance in *E. coli*”**

981 By Julia Bos, Yasmina Abou Haydar, Olena Mayboroda, Pierre Henri Commere and Didier
982 Mazel.

- 983
- 984 • Includes 2 tables, 10 figures and 4 movies
- 985

986
987
988
989
990
991
992
993
994
995
996
997
998
999
1000
1001
1002
1003
1004
1005
1006
1007
1008
1009
1010
1011
1012
1013
1014
1015
1016
1017
1018
1019
1020
1021
1022
1023
1024
1025
1026
1027
1028

1029 **Table S1** – List of strains used in this study.
 1030

Strain name	Genotype	Reference
wt	MG1655 (wt)	Lab collection
<i>ompA</i>	MG1655 $\Delta ompA::kan$	Lab collection
HD pPrcaA-gfp	BW25113 pPrcaA-gfp (<i>Kan</i>) Horizon Discovery <i>E. coli</i> gfp promoter collection # PEC3876-98156054	This study
wt pPrcaA-gfp	MG1655 (wt) pPrcaA-gfp (<i>Kan</i>)	This study
<i>ompA</i> pPclifim	W3110 (wt) $\Delta ompA::kan$ pPclifim (<i>spec</i>)	Ref ⁵⁰
UPEC	<i>E. coli</i> UPEC (wt) UGB554 CFP073	Gift from JM Ghigo's lab

1031
 1032
 1033
 1034
 1035

1036 **Table S2** – Concentrations of EVs and ratios EV counts per cell.
 1037

1038 **A**

EV donor cell and growth condition			CFUs/ml	EVs/ml	Mean Ratio EV/cell (Physiological)
Exponential	wt	mean	2.8 E+08.	9.47 E+08	0.21
		stdev.	5.6 E+07	4.5 E+08	
	wt+Pmb (0.4x)	mean	3.2 E+07	1.4 E+10	436
		stdev.	9.3 E+06	3.3 E+09	
	<i>ompA</i>	mean	4,69 E+08	n.d.	n.d.
		stdev.	1.9 E+07		
Stationary	wt	mean	3.17 E+09	1.24E+10	3.92
		stdev.	1.3 E+09	1.79 E+10	
	wt+Pmb (0.4x)	mean	2.1 E+09	1.4 E+11	67
		stdev.	1.3 E+09	1.9 E+11	
	<i>ompA</i>	mean	2.3 E+09	2.55 E+11	111
		stdev.	8.0 E+08	1.17 E+12	

1039
 1040
 1041
 1042
 1043
 1044
 1045
 1046
 1047
 1048
 1049
 1050
 1051
 1052
 1053
 1054
 1055

1056 **B**

Addition of pure EVs	Mean Ratio EV/cell (cell growth assays)	Mean Ratio EV/cell (uptake assays)
EV _{ompA}	161	72
EV _{wt}	7.8	3.5
EV _{wt+Pmb}	91	41

1057
 1058
 1059
 1060
 1061
 1062
 1063
 1064

1065 **Table S2** – Concentrations of EVs and ratios EV counts per cell. **A.** Mean and standard
 1066 deviations of cell counts (CFUs per ml) and EV concentrations (per ml) are reported across
 1067 strains and conditions of growth (exponential phase, stationary phase, that are used in this
 1068 study. EV concentrations were measured using a nano flow cytometer (Nanofcm technology).
 1069 Means of EV/cell ratio are indicated. **B.** Means of EV/cell ratio calculated for three types of
 1070 pure EVs used in cell growth assays and EV uptake assays. The origin of the EVs is indicated
 1071 (*ompA*, wt, wt+Pmb cells cultured overnight). Typically, for a growth assay in microplate, we
 1072 used 5 μ l EV_{ompA} or EV_{wt} or EV_{wt+Pmb} (from stationary phase culture) mixed with 2.5 μ l wt cells
 1073 (from stationary phase culture), and for the uptake assays, we used 40 μ l EV_{ompA} or EV_{wt} or
 1074 EV_{wt+Pmb} (from stationary phase culture) mixed with 0.5 ml of wt cells (exponential phase).

1075
1076
1077
1078
1079
1080
1081
1082
1083
1084
1085
1086
1087
1088
1089
1090
1091
1092
1093
1094
1095
1096
1097
1098
1099
1100
1101
1102
1103
1104
1105
1106
1107
1108
1109
1110
1111
1112
1113
1114
1115
1116
1117
1118
1119

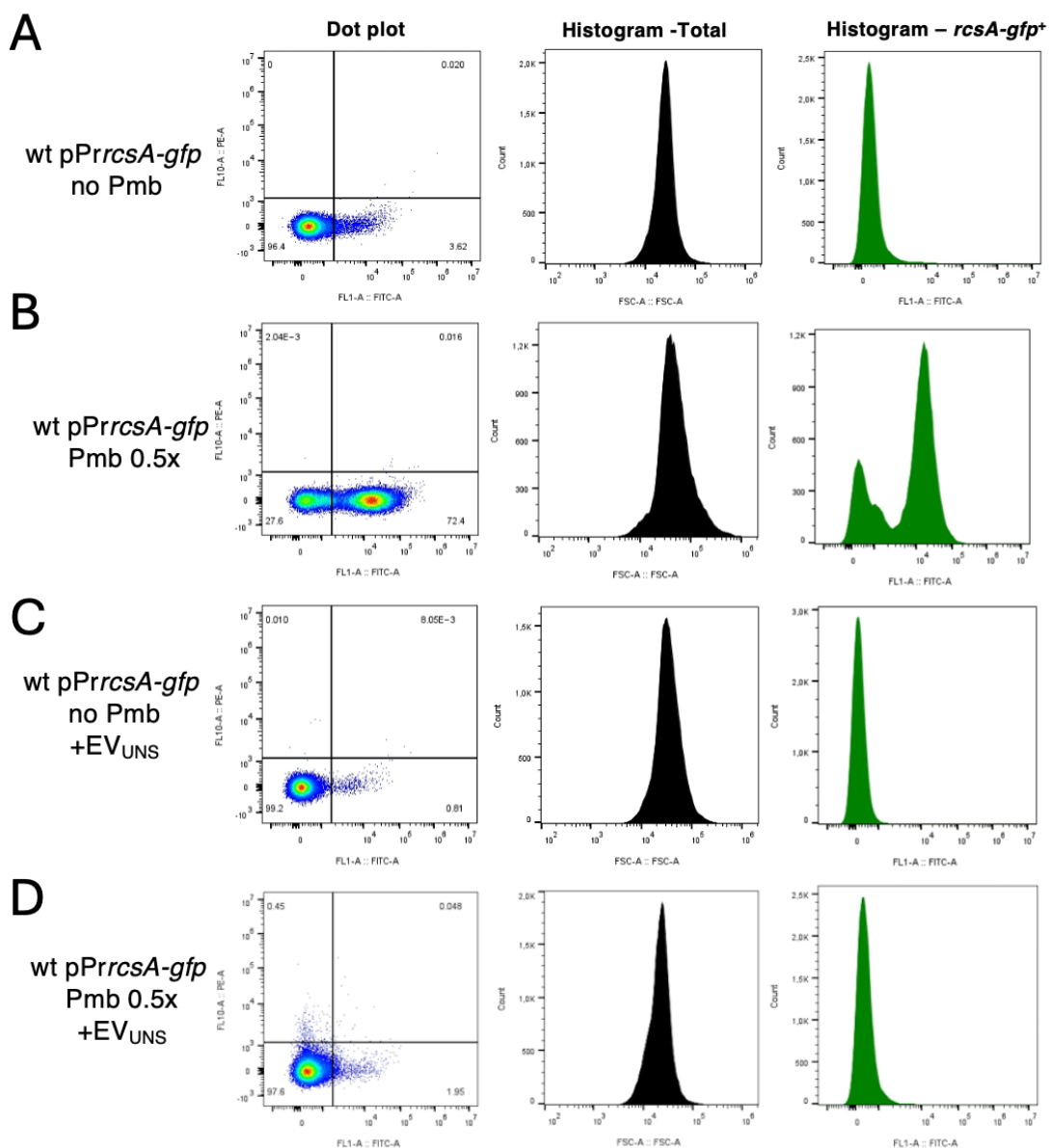


Figure S1: Pmb-induced *rcsA-GFP* expression in wt cells. Representative histograms and dot plots show *rcsA-gfp* expression, serving as a proxy for envelope stress response, analyzed by flow cytometry. Fractions of live cells grown in LB without antibiotics (A and C) or challenged with Pmb (0.5x MIC) (B and D) and/or pure EVs (added to a concentration of $\sim 1 \times 10^{10}$ EVs; ~ 72 EVs/cell), not fluorescent “unstained, UNS”, conc) (C and D), for 30 minutes were identified and gated for intracellular fluorescence analysis (FITC channel), associated with envelope stress response. Forward scatter (FSC) signal analysis provided information on cell size (total population). Refer to the “Methods” section in the main text for details on the methodology

1120
 1121
 1122
 1123
 1124
 1125
 1126
 1127
 1128
 1129
 1130
 1131
 1132
 1133
 1134
 1135
 1136
 1137
 1138
 1139
 1140
 1141
 1142
 1143
 1144
 1145
 1146
 1147
 1148
 1149
 1150
 1151
 1152
 1153
 1154
 1155
 1156
 1157
 1158
 1159
 1160
 1161
 1162
 1163
 1164

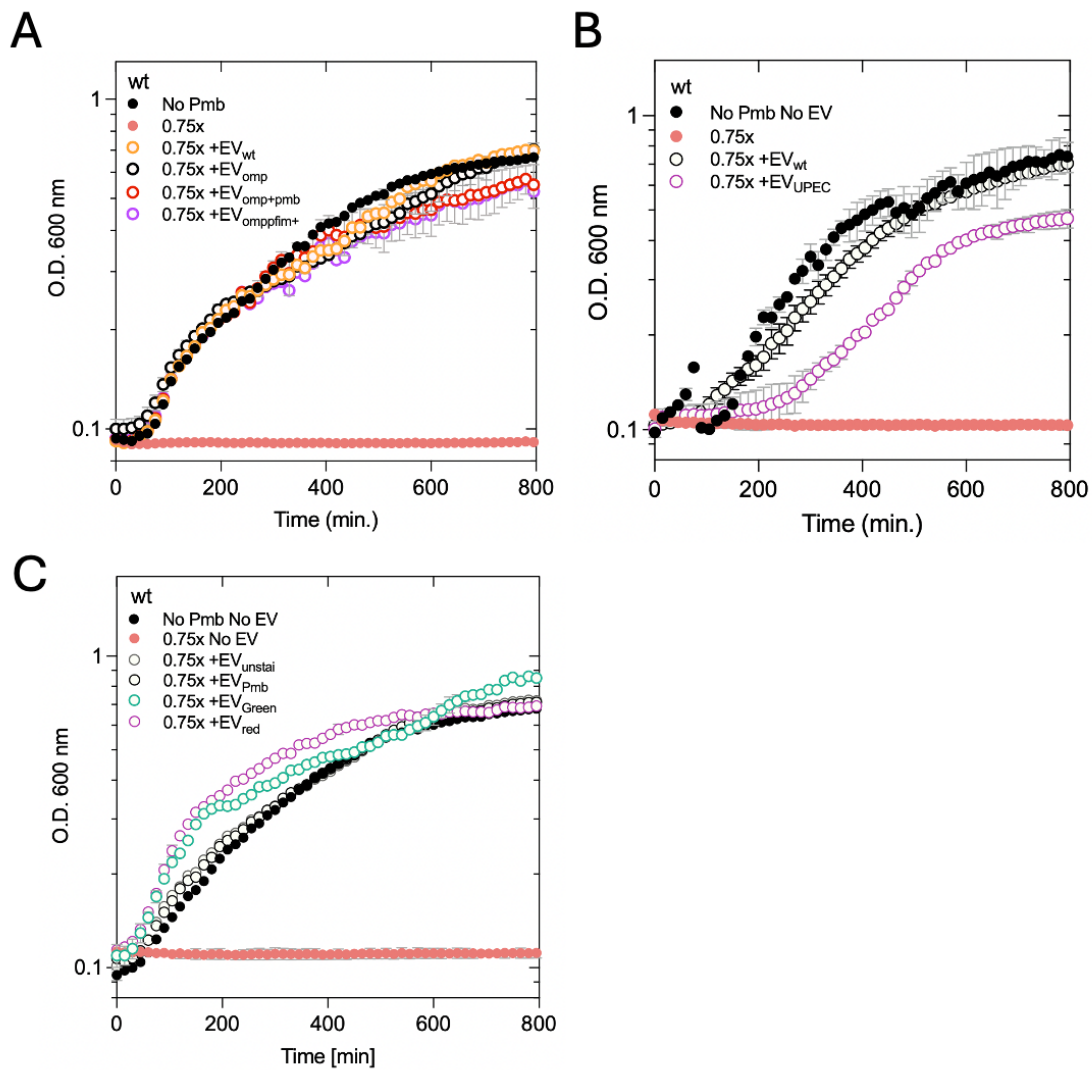


Figure S2: Growth restoration effect and cell protection against Pmb antibiotic by EVs of various origins. A. Effect of pure EVs (concentration normalized to 2.5 E+09 EV/ml) from different donor cells (wt, *ompA*, *ompA* +Pmb and hyper-fimbriated *ompA fim::Pclfim+*) on cell growth in the presence of Pmb (0.75x MIC). B. Effect of pure EVs from wt *E. coli* MG1655 and pathogenic *E. coli* UPEC (provided by JM Ghigo's lab), on cell growth under Pmb (0.75x MIC) conditions. C. Effect of EVs (concentration normalized to 2.5 E+09 EV/ml) with various fluorescent probes (FM1-43 (green), FM4-64 (red) and Pmb_{fl} which binds to EV membranes, on cell growth in the presence of Pmb (0.75x MIC).

1165
1166
1167
1168
1169
1170
1171
1172
1173
1174
1175
1176
1177
1178
1179
1180
1181
1182
1183
1184
1185
1186
1187
1188
1189
1190
1191
1192
1193
1194
1195
1196
1197
1198
1199
1200
1201
1202
1203
1204

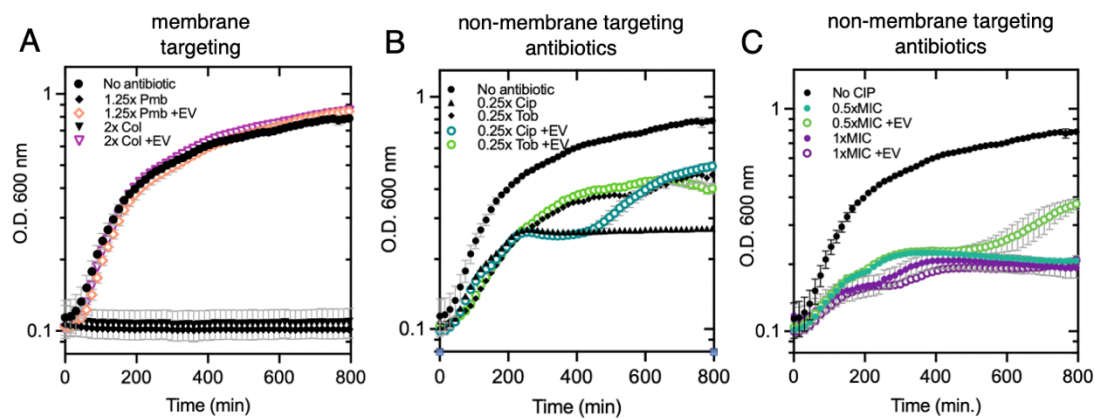


Figure S3: Effect of pure EVs on wt strain growth with membrane-targeting and non-membrane targeting antibiotics. **A.** cells cultured with membrane-targeting antibiotics at high doses (1.25x MIC Pmb and 2x Colistin) with or without EVs (from *ompA* donor cells, concentration normalized to 2.5E+09 EV/ml). **B-C.** cells cultured with non-membrane-targeting antibiotics at subMIC doses (0.25x (B) 0.5 xMIC cip (C) and 0.25x MIC tobra (B)) or MIC doses (1x MIC cip) (C), with or without EVs.

1205
 1206
 1207
 1208
 1209
 1210
 1211
 1212
 1213
 1214
 1215
 1216
 1217
 1218
 1219
 1220
 1221
 1222
 1223
 1224
 1225
 1226
 1227
 1228
 1229
 1230
 1231
 1232
 1233
 1234
 1235
 1236
 1237
 1238
 1239
 1240
 1241
 1242
 1243
 1244
 1245
 1246
 1247

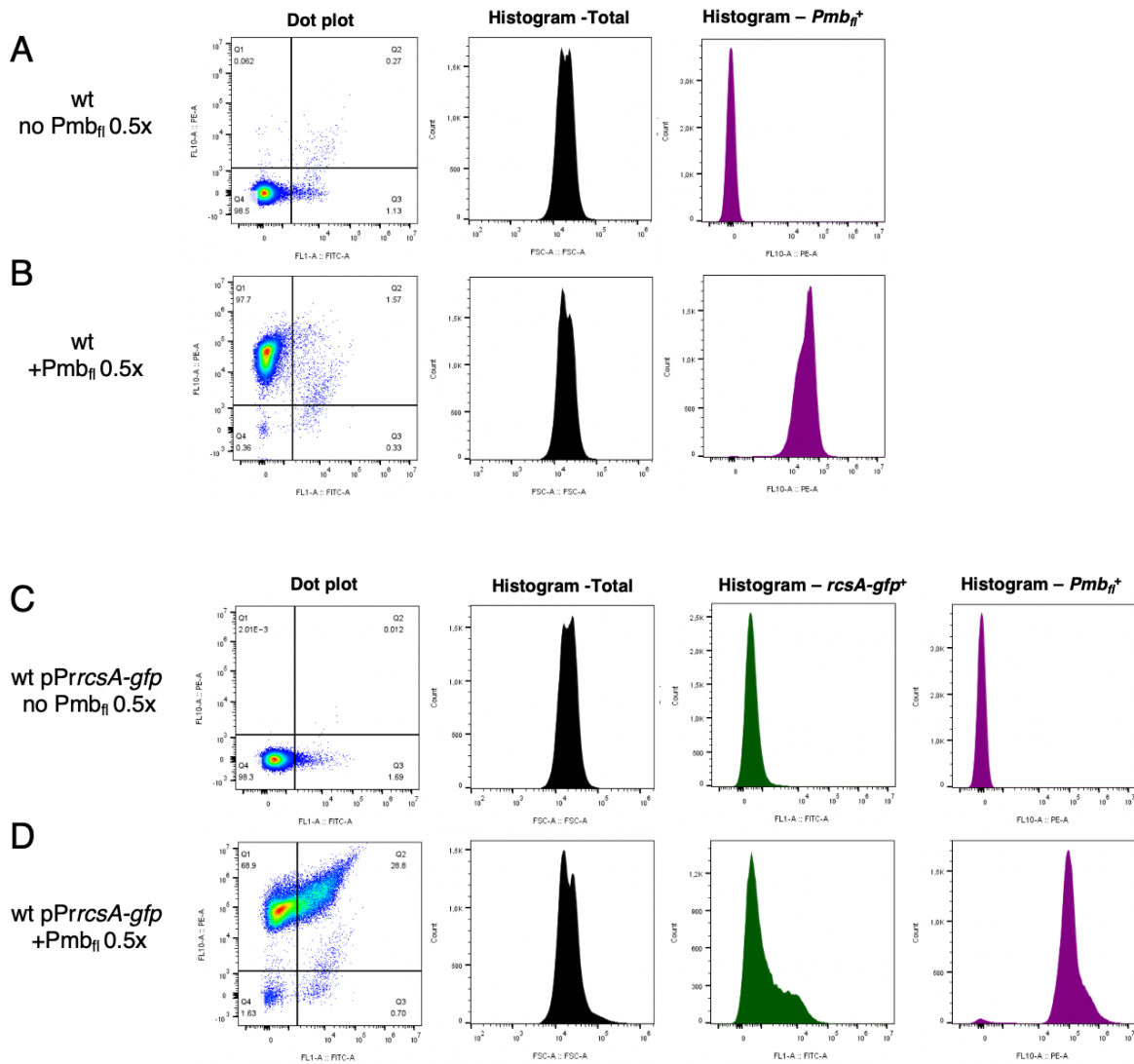


Figure S4: Pmb_{fl} insertion into cell membranes. Representative histograms and dot plots display Pmb_{fl} and *rccsA-gfp* fluorescence signals analyzed by flow cytometry. Subpopulations of live cells (wt or wt pPrccsA-gfp) either exposed or not exposed to Pmb_{fl} (0.5x MIC) for 30 min, were identified and gated for membrane fluorescence analysis with a PE laser (560 nm) (A-B-C-D) and for envelop stress response analysis using a FITC laser (488nm) (C-D). Forward scatter (FSC) signal analysis provided information on cell size (total population). Refer to the “Methods” section in the main text for further detailed methodology.

1248
 1249
 1250
 1251
 1252
 1253
 1254
 1255
 1256
 1257
 1258
 1259
 1260
 1261
 1262
 1263
 1264
 1265
 1266
 1267
 1268
 1269
 1270
 1271
 1272
 1273
 1274
 1275
 1276
 1277
 1278
 1279
 1280
 1281
 1282
 1283
 1284
 1285
 1286
 1287
 1288
 1289
 1290

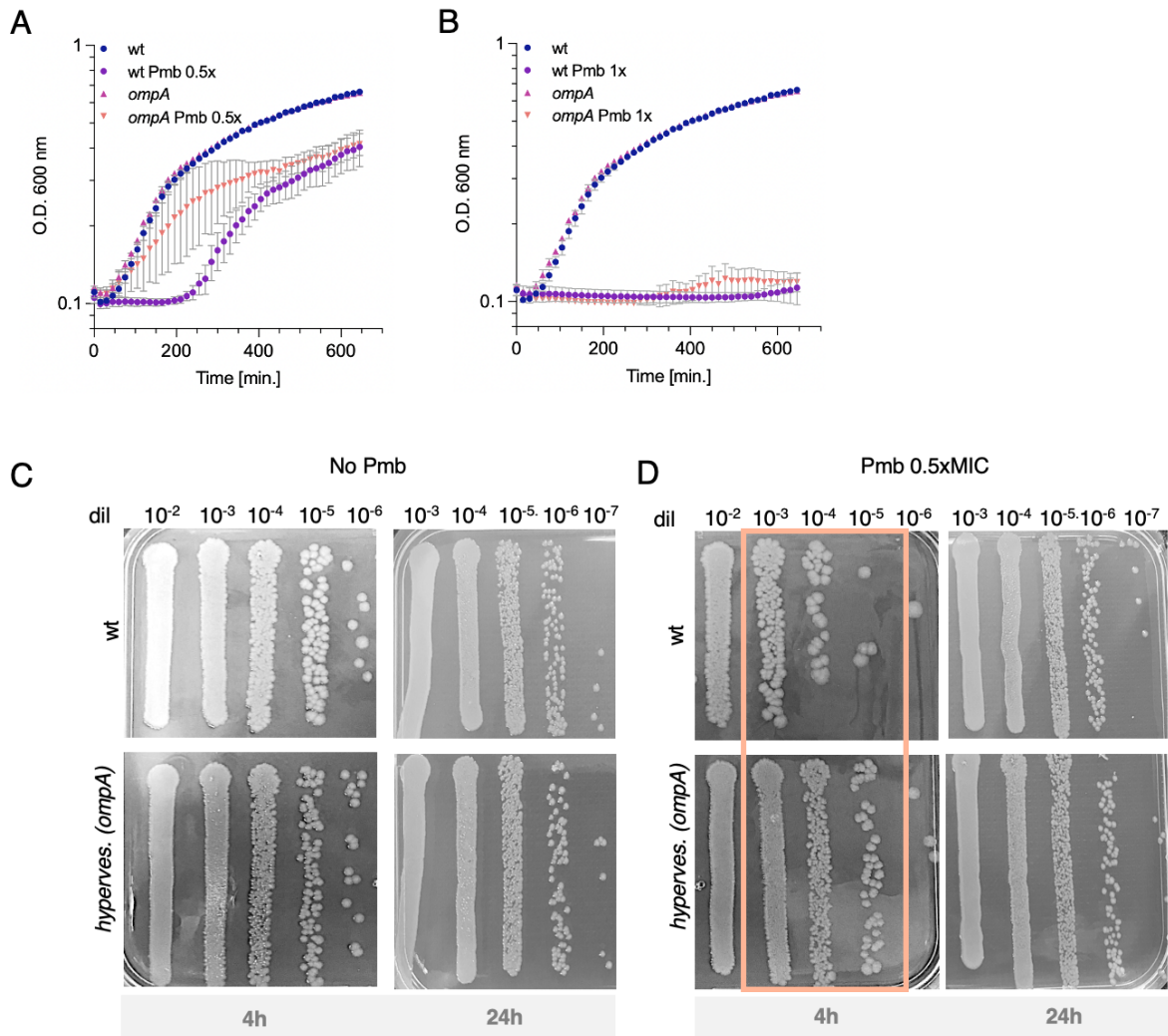


Figure S5: Growth curves and survival of wt and *ompA* strains in the presence or the absence of Pmb. When cultured in plain LB (no Pmb), the wt and *ompA* strains showed no significant differences in growth rate (A and B) or survival (C). The hypervesiculated *ompA* strain exhibits a growth (A) and survival (D) advantage (orange frame area) over the wt shortly after the addition of sub-MIC Pmb (0.5x MIC). However, this advantage is gone following prolonged treatment (24h) with sub-MIC Pmb (0.5x MIC) (D) or upon exposure to higher concentrations of Pmb (1x MIC) (B).

1291
1292
1293
1294
1295
1296
1297
1298
1299
1300
1301
1302
1303
1304
1305
1306
1307
1308
1309
1310
1311
1312
1313
1314
1315
1316
1317
1318
1319
1320
1321
1322
1323
1324
1325
1326
1327
1328
1329
1330
1331
1332
1333
1334
1335
1336

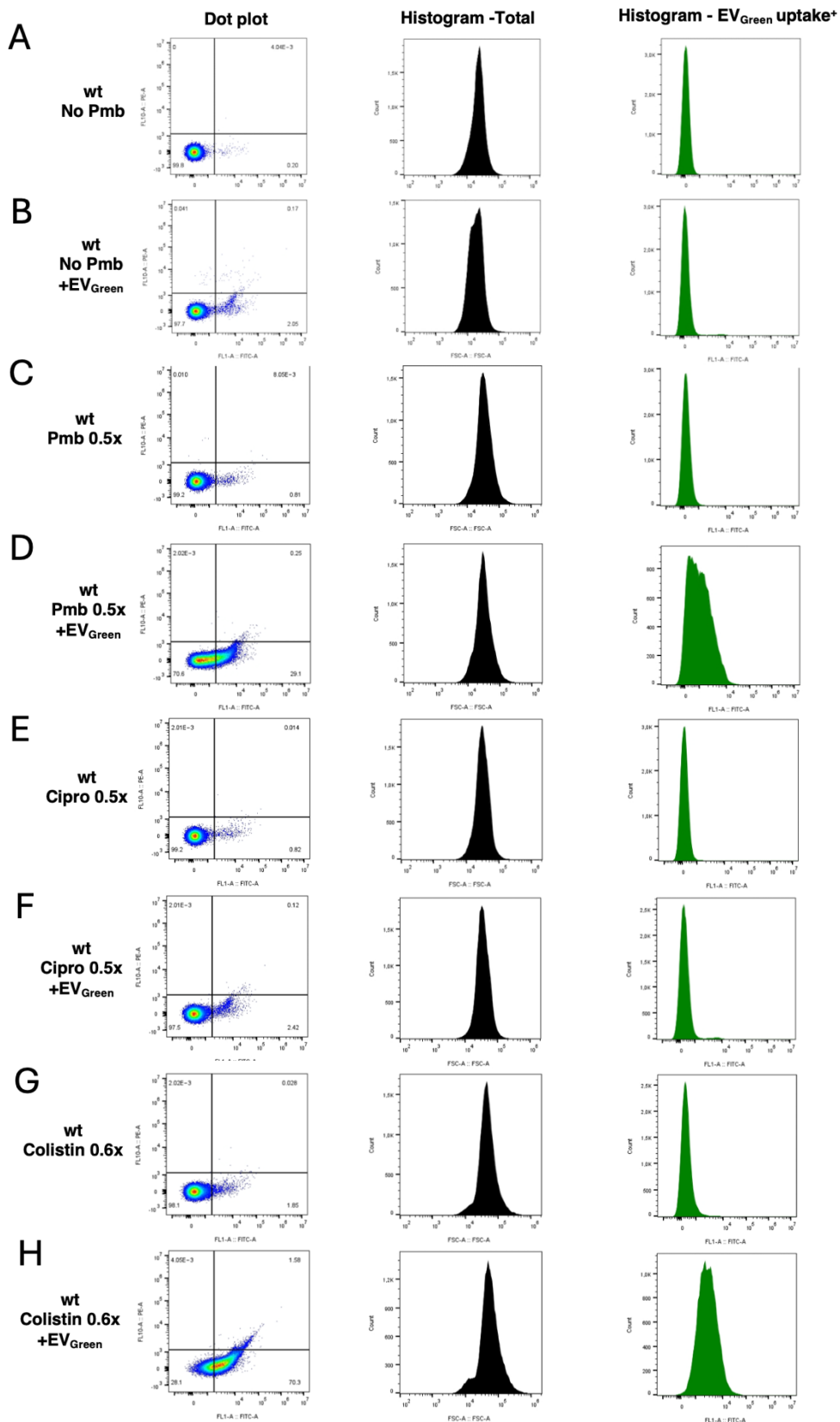


Figure S6: EV uptake efficacy varies with the type of antibiotic. Representative histograms and dot plots showing EV uptake signals at cell membranes analyzed by flow cytometry. Subpopulations of live wt cells exposed to either no drug treatment (A and B) or treated with Pmb (0.5x MIC; 30 min) (C and D), Ciprofloxacin (0.5x MIC; 30 min) (E and F),

1337 Colistin (0.6x MIC; 30 min) (G and H). After these treatments, pure EV_{Green} (concentration of
1338 ~1x10⁺¹⁰ EVs; ~72 EVs/cell) were added for 10 min. Subpopulations were identified and gated
1339 for membrane fluorescence analysis (EV uptake) using a FITC laser 488 nm. Forward scatter
1340 (FSC) analysis provides information about the size of cells (total population). See the
1341 “Methods” section in the main text for further details on the methodology.
1342

1343

1344

1345

1346

1347

1348

1349

1350

1351

1352

1353

1354

1355

1356

1357

1358

1359

1360

1361

1362

1363

1364

1365

1366

1367

1368

1369

1370

1371

1372

1373
1374
1375
1376
1377
1378
1379
1380
1381
1382
1383
1384
1385
1386
1387
1388
1389
1390
1391
1392
1393
1394
1395
1396
1397
1398
1399
1400
1401
1402
1403
1404
1405
1406
1407
1408
1409
1410
1411

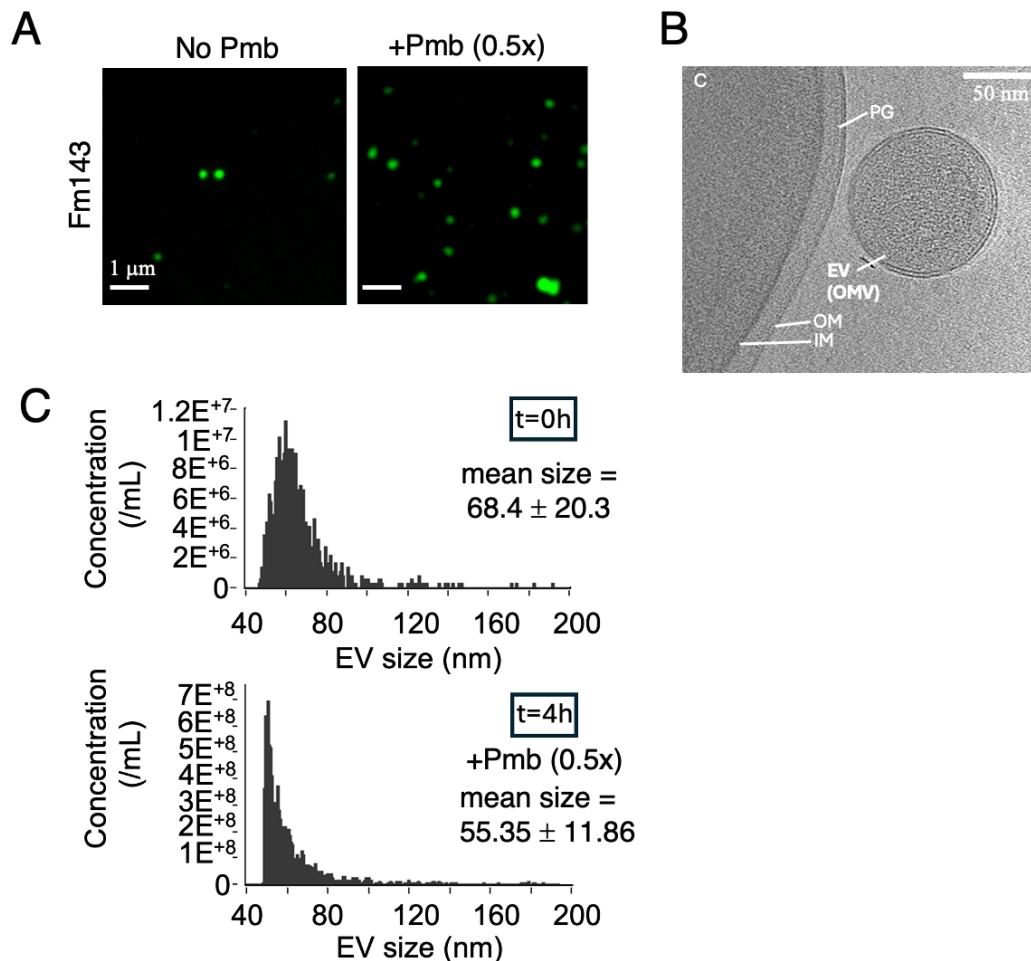


Figure S7: Visualization and quantification of EV production in the presence or absence of Pmb. A. Snapshots fluorescence images of purified EVs labeled with green lipophilic dye (Fm143) and immobilized on agarose pads mounted on a glass slide. EVs were purified from wt donor cells cultured in LB with or without Pmb 0.5x MIC for 20 hours. An increase in EV particles is detected in the presence of Pmb. B. Cryo-electron image of an EV (here an outer membrane vesicle OMV) produced by wt cells cultured in LB without Pmb. The cytoplasm (C), inner (IM) and outer (OM) membranes, and the peptidoglycan (PG) mesh are indicated. C. Size distribution of EVs (in nm). EV samples were purified from wt cells, cultured to the exponential phase (OD=0.5) (t = 0) then challenged for 4 hours with Pmb 0.5x MIC. The mean EV size and standard deviation are indicated. Data were obtained with a nanoflow cytometer (NanoFCM Technology).

1412
1413
1414
1415
1416
1417
1418
1419
1420
1421
1422
1423
1424
1425
1426
1427
1428
1429
1430
1431
1432
1433
1434
1435
1436
1437
1438
1439
1440
1441
1442
1443
1444
1445
1446
1447
1448
1449
1450
1451
1452
1453
1454
1455
1456
1457
1458
1459
1460
1461
1462

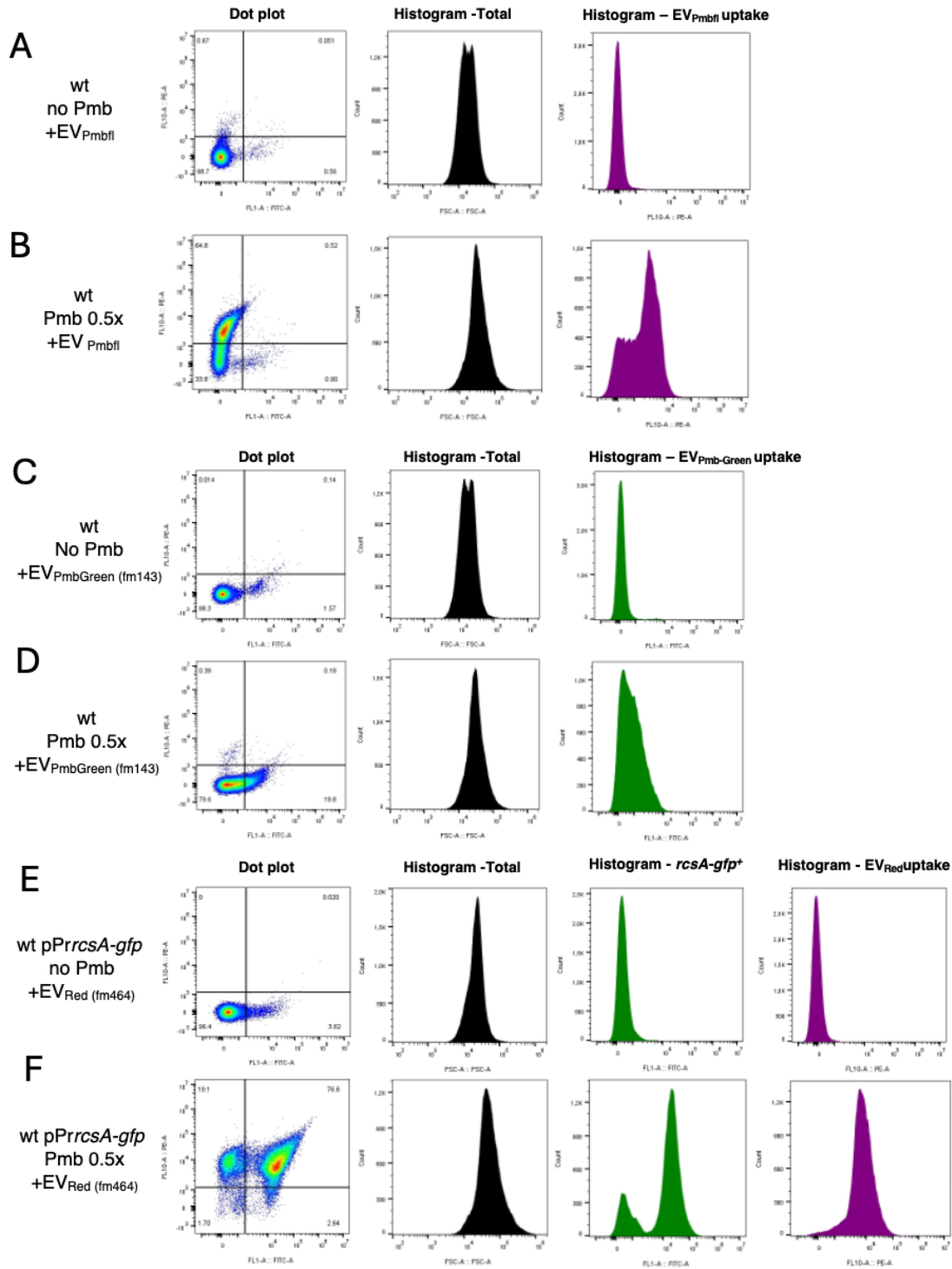


Figure S8: EV uptake occurs with EVs of different origins and fluorescent probes. Representative histograms and dot plots of EV uptake signals at cell membranes analyzed by flow cytometry. Subpopulations of live cells were exposed to either no drug treatment (A, C and E) or Pmb (0.5x MIC; 30 min) (B, D and F), followed by the addition of pure antibiotic-loaded EVs such as EV_{Pmbfl} (EVs purified from *ompA* cells grown with Pmb_{fl} 0.16x MIC for 20 hours) (A and B) or EV_{PmbGreen} (purified from *ompA* cells grown with Pmb 0.25x MIC for 20 hours) (C and D) and regular EVs stained with Fm464 (EV_{Red}) (E and F). All EVs were added to a concentration of $\sim 1 \times 10^{10}$ EVs; ~ 72 EVs/cell. These subpopulations were identified and gated for membrane fluorescence analysis using FITC 488 nm or PE (560 nm) lasers. Forward scatter (FSC) analysis provided information on cell size (total population). See the “Methods” section in the main text for detailed methodology.

1463
1464
1465
1466
1467
1468
1469
1470
1471
1472
1473
1474
1475
1476
1477
1478
1479
1480
1481
1482
1483
1484
1485
1486
1487
1488
1489
1490
1491
1492
1493
1494
1495
1496
1497
1498
1499
1500

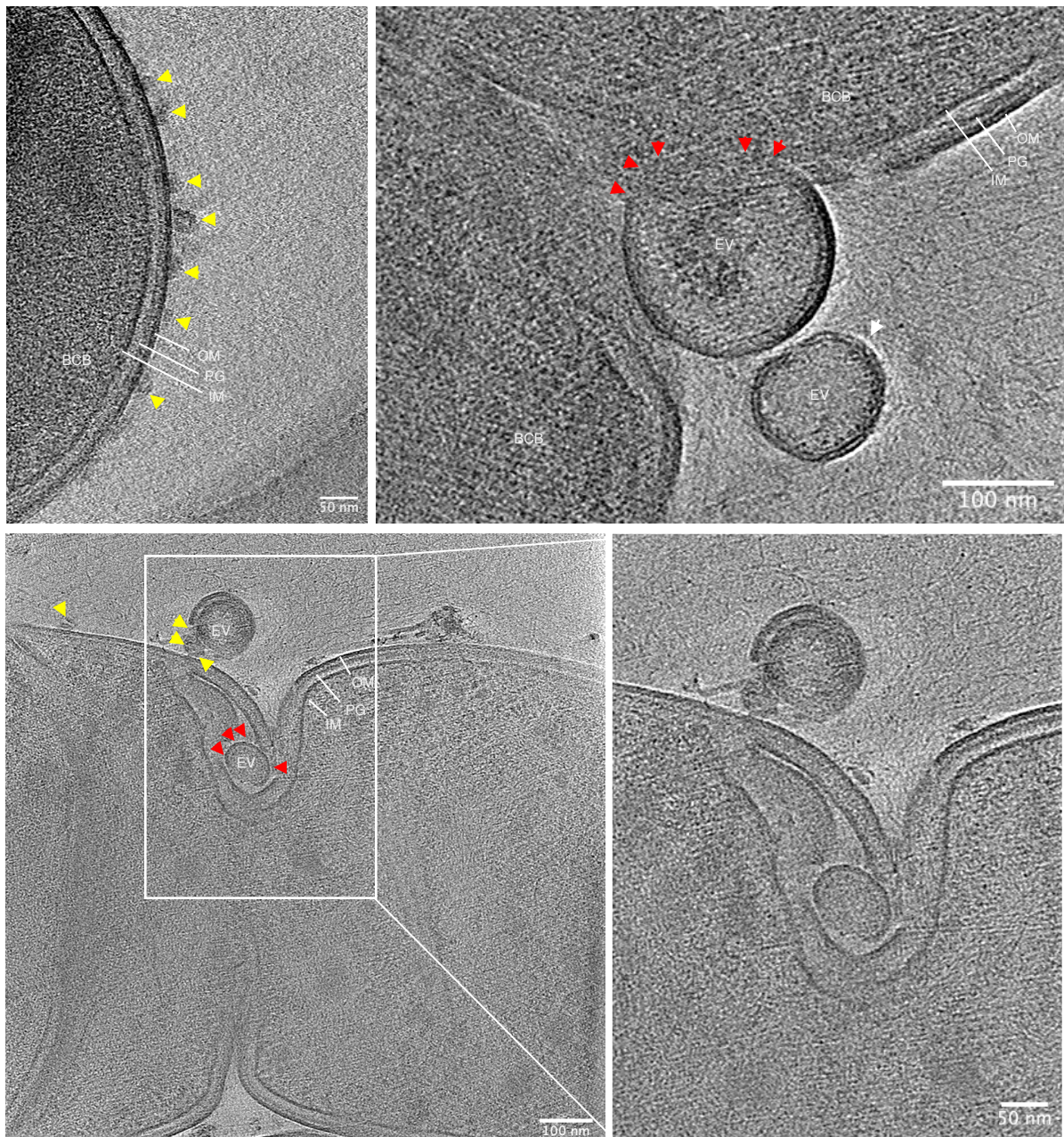


Figure S9: Cryo-electron images highlighting EV uptake at the membranes of *E. coli* cells challenged with Pmb (Refer to the Methods section in the main text for detailed methodology). Scale bar is indicated. The bacterial cell bodies (BCB) are indicated along with the outer (OM) and inner (IM) membranes of the cell, the intermembrane peptidoglycan (PG) mesh, and the EVs in proximity to- (white arrow), adhering (yellow arrow) or fused (red arrow) to the outer membrane.

1501
 1502
 1503
 1504
 1505
 1506
 1507
 1508
 1509
 1510
 1511
 1512
 1513
 1514
 1515
 1516
 1517
 1518
 1519
 1520
 1521
 1522
 1523
 1524
 1525
 1526
 1527
 1528
 1529
 1530
 1531
 1532
 1533
 1534
 1535
 1536
 1537
 1538
 1539
 1540
 1541
 1542

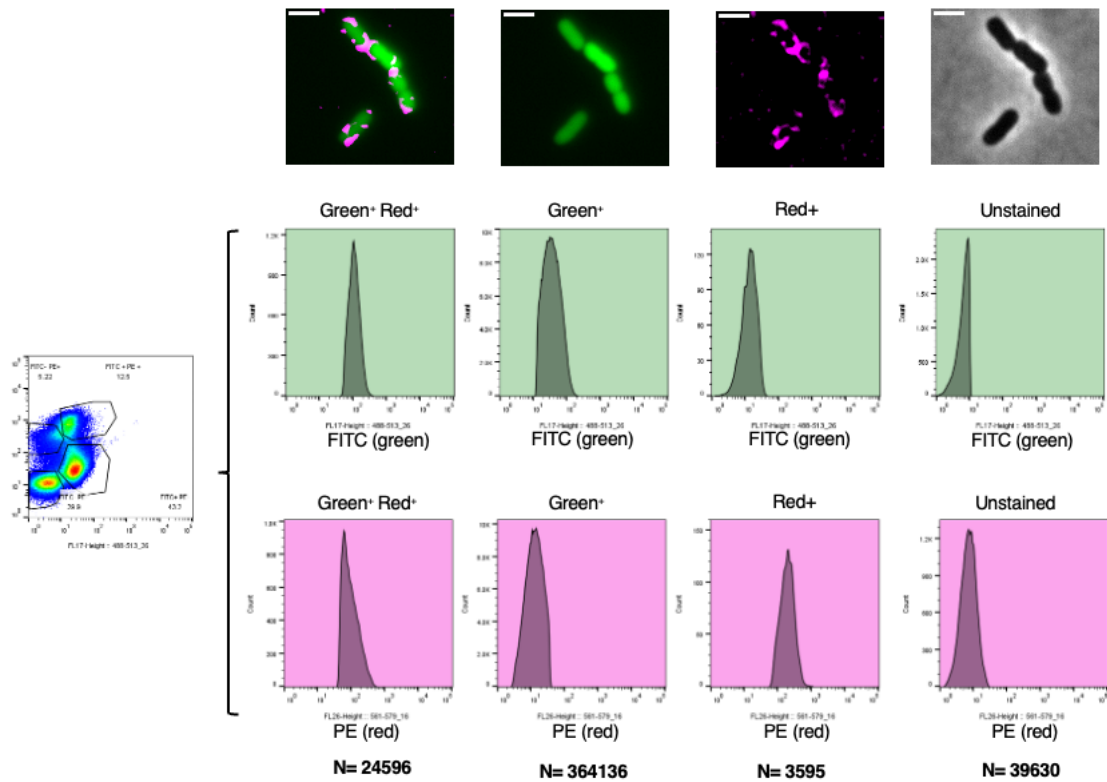


Figure S10: Cell sorting of EV-patched cells for growth recovery. Wild-type *pPracsA-gfp* cells were grown for 30 minutes in the presence of Pmb at 0.5× MIC. Pure EV_{Red} was then added to a final concentration of approximately 1×10^{10} EVs (~72 EVs per cell) for 10 minutes (see Methods: “Sample preparation for EV uptake analysis”). Cells were sorted based on fluorescence intensity using the following gating criteria: FITC for *rcaA-gfp* positive cells (‘stressed’ cells), PE for EV_{Red}-positive cells (‘patched’ cells), FITC + PE for EV_{Red} + *rcaA-gfp* positive cells (‘patched stressed’ cells), and unstained (non-fluorescent) cells. The number of sorted cells (N) in each gate is indicated. Fluorescence and phase-contrast microscopy images of the gated subpopulations after sorting are provided. Scale bar: 2 μ m.

1543 **4 movies**

1544

1545 **Movie S1:** vesiculation in wt cells promotes clearance of Pmb_{fl}-damaged membrane. Scale
1546 bar is 2 microns.

1547

1548

1549

1550

1551

1552

1553

1554

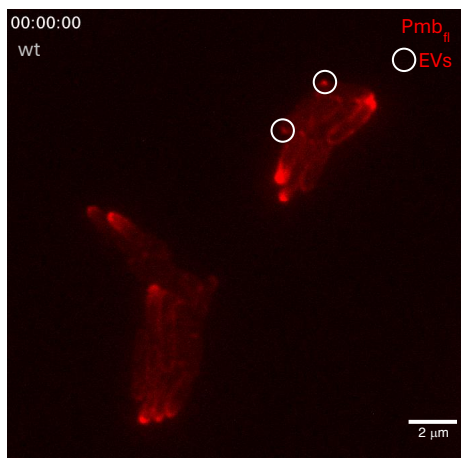
1555

1556

1557

1558

1559



1560

1561

1562 **Movie S2 :** vesiculation in *ompA* cells promotes clearance of Pmb_{fl}-damaged. Scale bar is 2
1563 microns.

1564

1565

1566

1567

1568

1569

1570

1571

1572

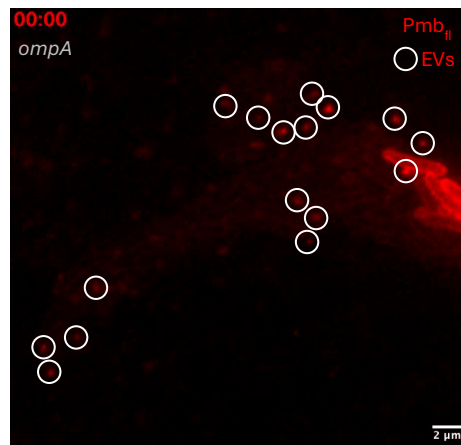
1573

1574

1575

1576

1577



1578

1579

1580 **Movie 3:** 3D Reconstructed tomogram of EV interaction with *E. coli* cell membrane in the
1581 absence of Pmb treatment. (see Figure 4C for corresponding image)

1582

1583 **Movie 4:** 3D Reconstructed tomogram of EV interaction with *E. coli* cell membrane in the
1584 absence of Pmb treatment. (see Figure 4D for corresponding image)

1585